Journal of Chemical&Engineering Data

pubs.acs.org/jced Article

Comprehensive Physicochemical Investigation of a Water-Soluble Adduct of C_{70} with L-Methionine and L-Cysteine

Konstantin N. Semenov,* Ali Mlhem, Alexander V. Akentiev, Dmitry A. Nerukh, Natalia V. Petukhova, Kirill V. Timoshchuk, Yuri Anufrikov, Gleb O. Iurev, Andrey V. Petrov, Igor V. Murin, Nikolay A. Charykov, Dilafruz K. Kholmurodova, Dilfuza Kiyamova, Perxan Aytmuratova, Maftuna Esanova qizi, and Vladimir V. Sharoyko*

Cite This: https://doi.org/10.1021/acs.jced.5c00615 Read Online

ACCESS | Metrics & More | Article Recommendations | Supporting Information

ABSTRACT: We study the physicochemical and biological properties of water-soluble adducts of fullerene C_{70} with L-methionine (C_{70}-Met, $C_{70}(C_5H_{11}NO_2S)_3$) and L-cysteine (C_{70}-Cys, $C_{70}(C_3H_7NO_2S)_3$). The adducts were characterized using ^{13}C NMR, IR, and UV spectroscopy, elemental analysis, and HPLC. The measured physicochemical properties included temperature and concentration dependence of density, viscosity, refraction, electrical conductivity, surface tension of aqueous solutions, solubility in binary systems (C_{70}-Met−H_2O and C_{70}-Cys−H_2O) and ternary systems (C_{70}-Met−NaCl−H_2O and C_{70}-Cys−NaCl−H_2O), as well as determination of the partition coefficient in an *n*-octan-1-ol−water system. In addition, investigation of binding to human serum albumin and DNA was conducted as well as antiradical activity in the model reaction with a stable 2,2-diphenyl-1-picrylhydrazyl radical (DPPH) was studied.

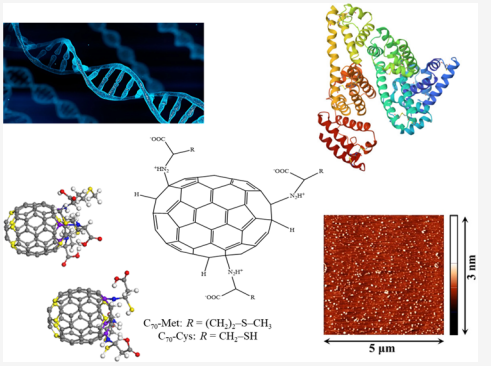

1. INTRODUCTION

Fullerenes are considered promising carbon-based nanomaterials with a wide potential for application in biomedicine due to their antioxidant,[1] antimicrobial,[2] antiviral,[3,4] membranotropic,[5] antitumor,[6] neuroprotective,[7,8] and photodynamic[9,10] properties. These characteristics make fullerenes suitable candidates for the development of advanced medical materials, particularly as components of targeted drug delivery systems.[11−13] However, their practical use is limited by their low solubility in water and aqueous solutions.[14,15] Therefore, surface functionalization using oxygen-containing groups[16,17] or biologically active compounds such as amino acids, peptides, and targeting vectors[18−25] is crucial for further biomedical applications. It is well-known that the physicochemical study of biologically active substances and their solutions plays a key role in preclinical research, providing essential data on biocompatibility and bioactivity in model systems.

Literature analysis shows that to date physicochemical studies of fullerenes and their adducts with amino acids and peptides mainly included computer modeling of physicochemical and thermodynamic properties of solids and aqueous solutions.[26−28] Computational approaches predominantly focused on elucidating the mechanisms and energetics of adduct formation and their association behavior in aqueous solutions.[29−37]

Experimental investigation of their thermodynamic properties includes measurements of the heat capacity and the calculation of thermodynamic functions of fullerene C_{60} adducts over a wide temperature range. To date several adducts have been studied, including C_{60}-Arg,[18] C_{60}-Lys,[19] and C_{60}-Hyp.[38] Investigations of aqueous solutions of these adducts included the analysis of concentration- and temperature-dependences of density, heat capacity, refractive index, electrical conductivity, viscosity, size distribution of associates, electrophoretic mobility, and solubility in binary and ternary systems.[17,19,20]

This work presents the results of physicochemical and biological studies of fullerene C_{70} adducts with L-methionine (C_{70}-Met, $C_{85}H_{33}N_3O_6S_3$) and L-cysteine (C_{70}-Cys, $C_{79}H_{21}N_3O_6S_3$). The physicochemical properties of C_{70}-Met and C_{70}-Cys solutions included temperature and concentration dependence of the density, viscosity, refraction, electrical conductivity, surface tension of aqueous solutions, and solubility in binary systems (C_{70}-Met−H_2O and C_{70}-Cys−H_2O). Additionally, the distribution of C_{70}-Met and C_{70}-Cys in

Received: September 24, 2025
Revised: November 24, 2025
Accepted: December 31, 2025

n-octanol−water systems, phase equilibria in the binary systems C_{70}-Met−H_2O, C_{70}-Cys−H_2O and the ternary systems C_{70}-Met−NaCl−H_2O, C_{70}-Cys−NaCl−H_2O were investigated. Furthermore, biocompatibility studies including interactions with human serum albumin (HSA) and DNA was carried out, as well as antiradical activity in a model reaction with DPPH was studied.

2. EXPERIMENTAL AND COMPUTATIONAL METHODS

2.1. Materials

C_{70}-Met and C_{70}-Cys were purchased from "MST Nano", St. Petersburg; the *n*-octan-1-ol sample was purchased from Sigma-Aldrich. The samples were used without further purification, and we have not performed separation of positional isomers of C_{70}-Met and C_{70}-Cys. The characteristics of the samples are given in Table 1.

Table 1. Characteristics of the Chemical Samples[a]

name	supplier	purity, kg·kg^{-1}	analysis method
n-octanol-1ol	Sigma-Aldrich	>0.985	gas chromatography
C_{70}-Met	MST nano	>0.995	liquid chromatography
C_{70}-Cys	MST nano	>0.995	liquid chromatography

[a]All uncertainties were estimated according to the Guide to the Expression of Uncertainty in Measurement (GUM).[39]

Deionized water was used (electrical conductivity was equal to 5.6×10^{-6} Sm^{1-}). For the preparation of aqueous solutions, purification of water was performed using a Millipore Simplicity UV apparatus (Merck KGaA, Germany). The aqueous solutions of C_{70}-Met and C_{70}-Cys were prepared by mixing the components at different proportions by mass using an electronic balance with ±0.0001 g precision. The solutions were stored in airtight glass stoppered bottles to prevent contamination and evaporation.

2.2. C_{70}-Met and C_{70}-Cys Characterization

To characterize the C_{70}-Met and C_{70}-Cys adducts, a set of physicochemical methods was used. The detailed description of the equipment is given in Table 2. The identification of C_{70}-Met and C_{70}-Cys is presented in the Supporting Information.

2.3. Physicochemical Investigation

Density, refraction, viscosity, electrical conductivity, surface properties of C_{60}-Met aqueous solutions were investigated according to the methods described in.[16,18−20,38,40−48] Methods and instruments used are listed in Table 2.

The solubility in C_{70}-Met−H_2O and C_{70}-Cys−H_2O binary systems in the temperature range 298.15 to 333.15 K was studied by isothermal saturation method as described in.[49] The same procedure was used for the investigation of solubility in C_{70}-Met−NaCl−H_2O and C_{70}-Cys−NaCl−H_2O ternary systems at 298.15 K.

The detailed methodology for determining the partition coefficients of fullerene adducts in the *n*-octan-1-ol−water system is presented in.[49]

For cryoscopy investigations of the C_{70}-Met−H_2O and C_{70}-Cys−H_2O binary systems, the concentration dependences of ice crystallization temperature were obtained. The ice crystallization temperatures were determined using a Beckman thermometer described in.[4,45,48,50]

The calculation of the electronic structures of C_{70}-Met and C_{70}-Cys was performed using the Materials Studio program. The DFT method implemented in the DMol3 program (PBE, DNP 4.4) in a water environment (COSMO model) was used to determine the charge states of atoms, total energy, and equilibrium geometry. To calculate the NMR spectra, CASTEP program of Materials Studio software package was used, which implements the DFT method on the basis of plane waves. Various functionals were used: LDA (CA-PZ),[51,52] PBE,[53] WC,[54] and PBESol[55] (GGA). The following calculation parameters were chosen: the cutoff energy for plane wave basis set was 550 eV, the total energy convergence criteria was 1×10^{-6} eV, pseudopotential "on the fly". The calculation cell was built as a simple cubic lattice with 20 Å side length. Classical molecular dynamics (MD) was performed using the FORCITE program for a box containing 1 molecule of C_{70}-Met or C_{70}-Cys and 1000 molecules of water, which was created using the Amorphous Cell module. The *NVT* ensemble was used at 298 K with the step size of 1 fs and the total simulation time of 1000 ps. The intermolecular interaction was parametrized using the calculated charges and equilibrium geometry using the short-range UFF potential (Universal Force Field).

Using molecular docking, the molecular interactions of C_{70}-Met and C_{70}-Cys with HSA were studied. Six binding sites in HSA molecule are known: IA, IIA, IIIA, IB, IIB, and IIIB.[56] HSA protein models with ligands at the corresponding binding sites were chosen as templates (4L9K, 5GIX, 2BXD, 3LU6, 2BXF, and 1E7A). HSA sequences were also obtained from the Protein Data Bank database. All steps of protein modeling, docking, and analytical calculations were performed using the Schrodinger molecular modeling package (version 2021−1, Schrödinger, LLC, New York, NY, 2021). The quality of the HSA models was checked and preprocessed in Protein Preparation Wizard (PPW).[57] The detected issues with invalid atom types (missing hydrogens, incorrect bond numbers), alternative positions, steric clashes, and other deviations were refined in PPW. Bond orders were assigned, and hydrogen atoms were added after removing the original hydrogens. Missing loops and side chains were checked with Prime,[58,59] and possible protonation states were generated with Epik using default parameters for pH 7.0 ± 2.0.[60] No issues were reported in the preprocessed protein structures (only some steric clashes remained since no additional MD relaxation was

Table 2. Methods and Instruments Used for Characterization, as Well as Physicochemical and Biological Study

method	equipment
identification of fullerene adducts	
CHNO−S elemental analysis	EuroVector EuroEA3000 (Italy)
solid-state ^{13}C NMR spectroscopy	Bruker instrument Avance III 400 WB (USA)
IR spectroscopy	FTIR08400S spectrometer (Japan)
dynamic light scattering, electrophoretic mobility	MalvernZetasizer 3000 instrument (Great Britain)
UV spectroscopy	SP-2000 spectrophotometer (Russia)
HPLC	Shimadzu LC-20 Prominence (Japan)
physicochemical investigation	
density	Anton Paar DMA 5000 M vibrating-tube densimeter (Austria)
refraction indexes	Anton Paar Abbemat multi-wavelength WR-MW Refractometer (Austria)
viscosity	Physica MCR 101 rotational rheometer (Austria)
electrical conductivity	Cyber Scan PC-300 measuring (Russia)
surface tension	KRUSS Microprocessor tensiometer K100 (Russia)
surface morphology	atomic force microscopy with the help of scanning probe microscope NTEGRA Prima (Russia)
biological activity	
antiradical activity (DPPH)	Bio Rad x Mark spectrophotometer (USA)
interaction with DNA	Beckman Coulter DU 800 spectrophotometer (USA)
binding to HSA	nano ITC 2G device (USA)
esterase activity of HSA	AMR-100T microplate reader spectrophotometer (China)
cytotoxicity	AMR-100T microplate reader spectrophotometer (China)

https://doi.org/10.1021/acs.jced.5c00615
J. Chem. Eng. Data XXXX, XXX, XXX−XXX

performed to avoid changing the binding site conformation with the bound ligand before the docking studies for proper mesh generation).

Docking was performed using the Glide package. The receptor grid was generated based on a cocrystallized ligand within the initial model. A grid of 30 × 30 × 30 Å with an inner core (20 × 20 × 20 Å) centered on the corresponding ligand was generated for the receptor. After grid generation, all prepared conformations were flexibly docked to the binding sites using the Glide XP (extra precision) method. Top poses of the compound in each binding site were selected for further evaluation based on various docking parameters such as docking score, binding energy, and bonding interactions analyzed in the Interaction Fingerprints panel. In order to refine the docking results, ligand binding energies were calculated for all obtained complexes using the MM/GBSA physical method.[61,62] The MM/GBSA free energy of binding (ΔG_{bind}) was calculated using the equation: $\Delta G_{bind} = E_{complex} - E_{ligand} - E_{receptor}$, where $E_{complex}$, E_{ligand}, and $E_{receptor}$ are the energetic calculations performed for a simple optimized MM/GBSA complex, an optimized free ligand, and an optimized free receptor. The best poses were selected based on the lowest MM-GBSA binding energy value. The calculations were performed using the OPLS4 force field and the VSGB solvation model.

The intermolecular interaction, association, and ^{13}C NMR spectra of C_{70}-Meth or C_{70}-Cys adducts were modeled for various isomers with Saturn-like distribution of amino acid residues using MD.

2.4. Biological Study

The antiradical activity of C_{70}-Met and C_{70}-Cys with a stable radical DPPH was studied according to the protocol presented in[20,48]

Interaction with DNA was studied using the spectrophotometric method. The UV absorption spectra of solutions of C_{70}-Met and C_{70}-Cys fullerene adducts and DNA (Fluka, USA) in the range of λ = 220−320 nm were recorded according to the method described in.[63]

Thermodynamic characterization of C_{70}-Met and C_{70}-Cys binding to HSA was carried out using a calorimetric titration method described in.[64] The influence of C_{70}-Met and C_{70}-Cys on the esterase activity of HSA in the model system with *p*-nitrophenyl acetate (NPA) was determined according to the method presented in.[65] It should be noted that these methods were validated for various carbon nanostructures (fullerene adducts,[63,65,66] graphene-based nanomaterials,[67,68] nanodiamonds[69]).

3. RESULTS AND DISCUSSION

3.1. Identification

Figure 1a shows the ^{13}C NMR spectrum of C_{70}-Met obtained using the CP/MAS method, which consists of the following signals: 140 ppm (carbon atoms of C_{70} bonded with L-Met), 180 ppm (carbon atom from carboxylic group of L-Met), 57 ppm (the sp^3-hybridized carbon atom of C_{70} bonded with the nitrogen atom of L-Met), 76 ppm (carbon atoms of C_{70} bonded with the hydrogen atoms), 63 ppm (α-carbon atom of L-Met), 38 and 16 ppm (carbon atoms of L-Met). Figure 1b shows the ^{13}C NMR spectrum of C_{70}-Cys obtained using the CP/MAS method with the following signals: 175 ppm (carbon atom in the carboxyl group of L-Cys), 75.1 ppm (α-carbon atom of L-Cys), 16 ppm (carbon atom in the $-CH_2-$ group of L-Cys), 60 ppm (sp^3-hybridized carbon atom of C_{70} bounded to nitrogen atom of L-Cys), 140 and 70 ppm (carbon atoms of C_{70} and carbon atoms of C_{70} bonded to the hydrogen atom, respectively).

The results of DFT modeling revealed that the most adequate agreement between the calculated and the experimental NMR spectra is for the isomer #4 (Table 10) in the PBE functional. At the same time, GGA functionals such as LDA, WC, and PBESol produced less satisfactory results. As can be seen in Figure 1, the chemical shifts for carbon atoms are in good agreement with experimental data for various

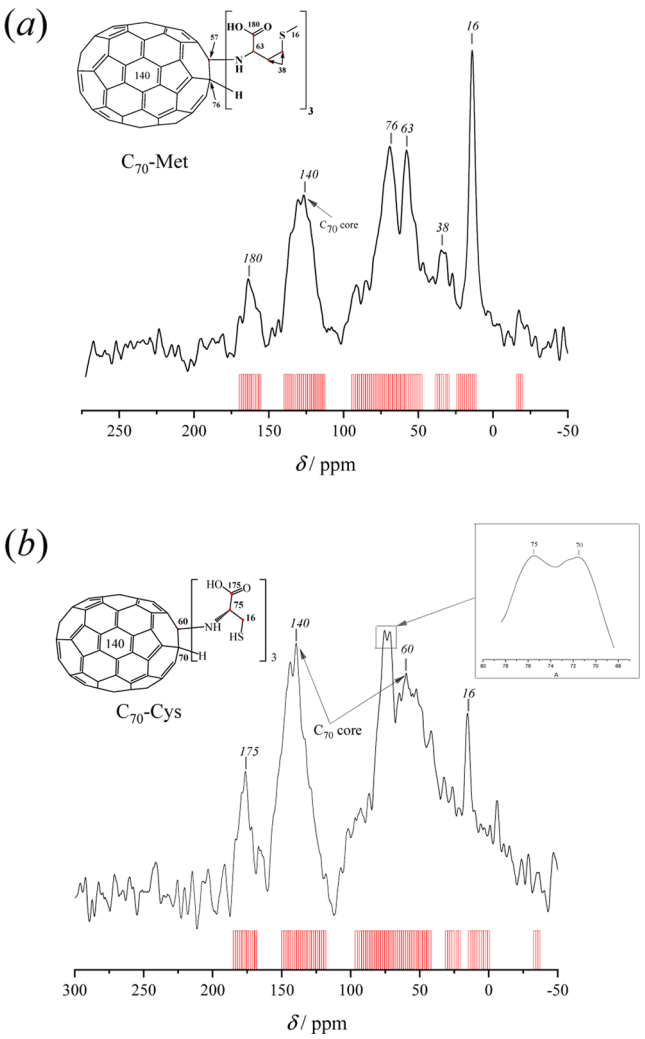

Figure 1. Experimental ^{13}C NMR spectra of C_{70}-Met (a) and C_{70}-Cys (b) obtained using CP/MAS method (solid black line) and calculated ^{13}C NMR spectra by the DFT method using the PBE functional (red bars). δ is the chemical shift.

characteristic bonds with homo- and heteroatoms in C_{70}-Met and C_{70}-Cys. Thus, the good applicability of this computational approach for the prediction of the C_{70}-Met and C_{70}-Cys NMR spectra is demonstrated (Figure 1).

Figure S1 shows the IR spectra of C_{70}-Met and C_{70}-Cys: 599.9 cm^{-1} (νC−C), 1398 cm^{-1} (νC−N), 1484 cm^{-1} (νC═O), 1847 cm^{-1} (δSN−H), 2920 cm^{-1} (νC−H), 3729 cm^{-1} (νO−H) for C_{70}-Met and 605.7 cm^{-1} (νC−C), 1396 cm^{-1} (νC−N), 1491 cm^{-1} (νC═O), 1846 cm^{-1} (δSN−H), 2923 cm^{-1} (νC−H), 3727 cm^{-1} (νO−H) for C_{70}-Cys.

Elemental analysis gives the following: C 79.4 ± 0.2%, H 2.5 ± 0.2%, N 3.1 ± 0.2%, S 7.4 ± 0.2% (exp.), C 79.2%, H 2.6%, N 3.3%, S 7.5% (calcd. for C_{70}-Met)and C 78.5 ± 0.2%, H 1.6 ± 0.1 ± 0.2%, N 3.3 ± 0.2%, S 7.8 ± 0.2% (exp.), C 78.8%, H 1.7%, N 3.5%, S 8.0%. (calcd. for C_{70}-Cys). The experimental data are in good agreement with the calculated values. Based on the results of the elemental analysis, it was established that fullerene C_{70} forms tris-adducts with L-Met ($C_{85}H_{33}N_3O_6S_3$) and L-Cys ($C_{79}H_{21}N_3O_6S_3$).

The purity of C_{70}-Met and C_{70}-Cys was determined by HPLC to be 97.2% for C_{70}-Met and 96.15% for C_{70}-Cys (Figure S2). As can be seen from Figure S2 the chromatograms

https://doi.org/10.1021/acs.jced.5c00615
J. Chem. Eng. Data XXXX, XXX, XXX−XXX

of C_{70}-Met and C_{70}-Cys consist of one peak, which indicates high purity of the obtained compound. The conditions of chromatographic analysis are presented in the caption of Figure S2.

The electronic spectra of C_{70}-Met and C_{70}-Cys aqueous solutions are shown in Figure S3. For comparison, the spectrum of fullerene C_{70} in *o*-xylene is shown. The absence of the absorption peak at λ = 472 nm (characteristic for pure C_{70}[70]) indicates transformation of C_{70} to the fullerene adducts.

3.2. Physicochemical Investigation of C_{70}-Met and C_{70}-Cys

3.2.1. Densities and Volume Properties of C_{70}-Met and C_{70}-Cys Water Solutions. Table 3 and Figure S4 show

Table 3. Temperature (T) and Concentration (C) Dependences of Density (ρ) of C_{70}-Met and C_{70}-Cys Aqueous Solutions at P = 0.1 MPa[a]

	T/K				
x	293.15	303.15	313.15	323.15	333.15
		ρ/kg·m^{-3}			
		C_{70}-Met			
$1.40\cdot10^{-7}$	998.20	995.65	992.22	988.05	983.22
$1.40\cdot10^{-6}$	998.24	995.69	992.26	987.96	983.24
$3.50\cdot10^{-6}$	998.31	995.76	992.33	988.15	983.32
$7.70\cdot10^{-6}$	998.45	995.89	992.46	988.28	983.45
$1.40\cdot10^{-5}$	998.63	996.08	992.64	988.47	983.63
$3.50\cdot10^{-5}$	999.28	996.72	993.28	989.10	984.26
$7.00\cdot10^{-5}$	1000.36	997.78	994.33	990.14	985.30
$1.40\cdot10^{-4}$	1002.55	999.96	996.50	992.28	987.41
$2.10\cdot10^{-4}$	1004.70	1002.08	998.60	994.38	989.51
		C_{70}-Cys			
$1.50\cdot10^{-7}$	998.20	995.65	992.22	988.05	983.22
$1.50\cdot10^{-6}$	998.25	995.70	992.27	988.09	983.26
$3.75\cdot10^{-6}$	998.32	995.77	992.34	988.17	983.33
$8.24\cdot10^{-6}$	998.46	995.91	992.49	988.31	983.48
$1.50\cdot10^{-5}$	998.70	996.14	992.71	988.53	983.69
$3.75\cdot10^{-5}$	999.41	996.85	993.41	989.23	984.39
$7.49\cdot10^{-5}$	1000.64	998.07	994.62	990.43	985.54
$1.50\cdot10^{-4}$	1003.10	1000.50	997.03	992.83	987.97
$2.25\cdot10^{-4}$	1005.26	1002.64	999.16	994.94	990.08

[a]Standard uncertainty: u(T) = 0.01 K, u(P) = 10 kPa. Combined expanded uncertainty for ρ is $Uc(\rho)$ = 0.01 kg·m^{-3} (095 level of confidence).

concentration dependences of density (ρ) of aqueous solutions of C_{70}-Met and C_{70}-Cys. The analysis of Figure S4 shows that the density values rise with the increase of concentration of C_{70}-Met and C_{70}-Cys. The concentration dependence of the average molar volume ($\bar{V}$) of solutions were calculated using eq 1

$$\bar{V} = V/(n_1 + n_2) \quad (1)$$

where summation is carried out for both components (1 is H_2O, 2 is C_{70}-Met or C_{70}-Cys) and V and n_i are the volume and the number of moles of the i-th component in 1 L of the solution. Concentration dependences of average molar volumes are presented in Figure S5.

The partial molar volumes of solution components V_i were calculated according to eqs 2 and 3

$$V_{H_2O} = \bar{V} - x_{C_{70}-adduct}(\partial\bar{V}/\partial x_{C_{70}-adduct})_{T,P} \quad (2)$$

$$V_{C_{70}-adduct} = \bar{V} - x_{H_2O}(\partial\bar{V}/\partial x_{H_2O})_{T,P} \quad (3)$$

where x_i is the mole fraction of the i-th component of the solution. The derivatives $(\partial V/\partial x_{C70\text{-}adduct})_{T,P}$ and $(\partial V/\partial x_{H2O})_{T,P}$ were calculated numerically. The concentration dependences of the partial molar volumes of solution are presented in Figures S6 and S7. Figure S7 shows that there is a significant decrease in the values of the partial molar volumes of C_{70}-Met and C_{70}-Cys in the region of dilute solutions. It proves that the addition of small portions of nanoparticles significantly compacts and structures the solution. The results are consistent with previously obtained data for other water-soluble fullerene derivatives: C_{60}-Gly,[20] C_{60}-Arg,[18] C_{60}-Thr,[43] C_{60}-Lys,[19] as well as carboxylated fullerene $C_{60}[C(COOH)_2]_3$[17] and polyhydroxylated fullerenes $C_{60}(OH)_{22-24}$ and $C_{70}(OH)_{12}$.[16,41]

3.2.2. Refraction of Aqueous Solutions of C_{70}-Met and C_{70}-Cys. Table 4 presents refraction indexes of C_{70}-Met and C_{70}-Cys aqueous solutions in the concentration range x = $1.40\cdot10^{-7}$–$2.25\cdot10^{-4}$ and T = 293.15 K. Using the Lorentz–Lorenz equation, the concentration dependences of the specific (r) and molar (R) refractions of C_{70}-Met and C_{70}-Cys solutions at 293.15 K were calculated

$$r = \frac{n_D^2 - 1}{(n_D^2 + 2)\cdot\rho} \quad (4)$$

$$R = \frac{(n_D^2 - 1)\cdot\bar{M}}{(n_D^2 + 2)\cdot\rho} \quad (5)$$

$$\text{where}\ \bar{M} = M_{H_2O}\cdot x_{H_2O} + M_{adduct}\cdot x_{adduct} \quad (6)$$

The concentration dependences of r and R for aqueous solutions are presented in Table 4. Obviously, the r and R values of C_{70}-Met and C_{70}-Cys adducts can be calculated using the refractions of water

$$r = (r_{H_2O}\cdot\omega_{H_2O} + r_{adduct}\cdot\omega_{adduct})\cdot(1/100) \quad (7)$$

$$R = R_{H_2O}\cdot x_{H_2O} + R_{adduct}\cdot x_{adduct} \quad (8)$$

The values of R_{adduct} and r_{adduct} for the C_{70}-Met are (3.04 ± 0.4)·10^{-4} m^3·mol^{-1} and (2.36 ± 0.3)·10^{-4} m^3·kg^{-1} and for C_{70}-Cys (3.06 ± 0.4)·10^{-4} m^3·mol^{-1} and (2.54 ± 0.3)·10^{-4} m^3·kg^{-1}, correspondingly. Due to the low accuracy of the refraction data at C_{adduct} < $3.75\cdot10^{-6}$ these values were not used for calculations.

The R_{adduct} values were additionally calculated using the Eisenlohr additivity rule at different spectral lines (Hα [λ = 658.3 nm] and Hγ [λ = 436.1 nm]).

$$R_{C_{70}-Met} \approx 70R_C + 3\cdot(5R_C + 11R_H + R_{N(-NH-)} + R_{O(-C=O)} + R_{O(-OH)} + R_{S(-S-)} + 33R \approx 70\cdot2.418 + 3\cdot(5\cdot2.418 + 11\cdot1.10 + 2.502 + 2.211 + 1.525 + 8.0) + 33\cdot1.733 \approx 341.73 \pm 5\ \text{cm}^3\cdot\text{mol}^{-1}\ (3.417\cdot10^{-4}\ \text{m}^3\cdot\text{mol}^{-1}),$$

$$R_{C_{70}-Cys} \approx 70R_C + 3\cdot(3R_C + 7R_H + R_{N(-NH-)} + R_{O(-C=O)} + R_{O(-OH)} + R_{S(-S-)} + 33R \approx 70\cdot2.418 + 3\cdot(3\cdot2.418 + 7\cdot1.10 + 2.502 + 2.211 + 2.525 + 8.0) + 33\cdot1.733 \approx 317.025 \pm 4\ \text{cm}^3\cdot\text{mol}^{-1}\ (3.17\cdot10^{-4}\ \text{m}^3\cdot\text{mol}^{-1}),$$

The specific refractions of C_{70}-Met and C_{70}-Cys were calculated according to eq 9

$$r_{C_{70}-Met} \approx R_{C_{70}-Met}/M_{C_{70}-Met} = 341.73/1287 \approx 0.2655 \pm 0.02\text{cm}^3\cdot\text{g}^{-1}(\approx 2.65\cdot10^{-4}\text{m}^3\cdot\text{kg}^{-1}) \quad (9)$$

https://doi.org/10.1021/acs.jced.5c00615
J. Chem. Eng. Data XXXX, XXX, XXX−XXX

Table 4. Refraction Properties of the C_{70}-Met and C_{70}-Cys Aqueous Solutions at T = 293.15 K[a,b]

x	n_D	$r/10^{-4}$•m^3·kg^{-1}	$R/10^{-6}$·m^3·mol^{-1}	$R_{adduct}/10^{-4}$ m^3·mol^{-1}	$r_{adduct}/10^{-4}$ m^3·kg^{-1}
			C_{70}-Met		
$1.40\cdot10^{-7}$	1.3330	2.0606	3.7091		
$1.40\cdot10^{-6}$	1.3330	2.0605	3.7093		
$3.50\cdot10^{-6}$	1.3330	2.0607	3.7101	3.0248	2.3496
$7.70\cdot10^{-6}$	1.3331	2.0608	3.7114	3.0290	2.3529
$1.40\cdot10^{-5}$	1.3332	2.0609	3.7133	3.0379	2.3598
$3.50\cdot10^{-5}$	1.3335	2.0614	3.7196	3.0488	2.3683
$7.00\cdot10^{-5}$	1.3341	2.0621	3.7301	3.0438	2.3644
$1.40\cdot10^{-4}$	1.3351	2.0636	3.7512	3.0427	2.3636
$2.10\cdot10^{-4}$	1.3362	2.0651	3.7723	3.0452	2.3655
			C_{70}-Cys		
$1.50\cdot10^{-7}$	1.3330	2.0606	3.7092		
$1.50\cdot10^{-6}$	1.3330	2.0606	3.7095		
$3.75\cdot10^{-6}$	1.3331	2.0607	3.7102	3.0248	2.5142
$8.24\cdot10^{-6}$	1.3331	2.0609	3.7116	3.0566	2.5407
$1.50\cdot10^{-5}$	1.3333	2.0611	3.7136	3.0610	2.5444
$3.75\cdot10^{-5}$	1.3336	2.0618	3.7204	3.0580	2.5419
$7.49\cdot10^{-5}$	1.3343	2.0630	3.7317	3.0598	2.5433
$1.50\cdot10^{-4}$	1.3357	2.0655	3.7545	3.0690	2.5510
$2.25\cdot10^{-4}$	1.3369	2.0679	3.7773	3.0738	2.5550

[a]Standard uncertainties are $u(T)$ = 0.03 K and $u(P)$ = 10 kPa and $u(n_D)$ = 0.00004 (0.95 level of confidence). [b]x is the mole fraction of C_{70}-Met and C_{70}-Cys, n_D is the refraction index; r and R are specific and molar refractions of aqueous solutions, $r_{C_{70}-adduct}$ and $R_{C_{70}-adduct}$ are specific and molar refractions of C_{70}-Met and C_{70}-Cys P = 0.1 MPa.

Table 5. Temperature (T) and Concentration Dependences of the Dynamic (η) and Kinematic (η_k) Viscosities of Aqueous Solutions of C_{70}-Met and C_{70}-Cys[a,b]

	T/K					T/K				
x	293.15	303.15	313.15	323.15	333.15	293.15	303.15	313.15	323.15	333.15
	η/mPa·s					η_k/mm^2·s^{-1}				
					C_{70}-Met					
$1.40\cdot10^{-7}$	1.004	0.800	0.657	0.552	0.474	1.006	0.803	0.662	0.558	0.482
$1.40\cdot10^{-6}$	1.004	0.800	0.657	0.552	0.474	1.006	0.803	0.662	0.559	0.482
$3.50\cdot10^{-6}$	1.003	0.800	0.659	0.552	0.474	1.005	0.803	0.664	0.559	0.482
$7.70\cdot10^{-6}$	1.006	0.802	0.659	0.554	0.476	1.007	0.805	0.664	0.561	0.484
$1.40\cdot10^{-5}$	1.007	0.803	0.659	0.555	0.479	1.008	0.806	0.663	0.561	0.487
$3.50\cdot10^{-5}$	1.015	0.809	0.664	0.558	0.479	1.016	0.812	0.669	0.564	0.487
$7.00\cdot10^{-5}$	1.028	0.819	0.672	0.565	0.485	1.028	0.821	0.675	0.570	0.492
$1.40\cdot10^{-4}$	1.048	0.834	0.684	0.575	0.493	1.046	0.834	0.686	0.579	0.499
$2.10\cdot10^{-4}$	1.070	0.851	0.697	0.585	0.502	1.065	0.849	0.698	0.589	0.507
					C_{70}-Cys					
$1.50\cdot10^{-7}$	1.005	0.801	0.657	0.553	0.476	1.007	0.804	0.663	0.560	0.484
$1.50\cdot10^{-6}$	1.004	0.800	0.656	0.552	0.474	1.006	0.803	0.661	0.558	0.482
$3.75\cdot10^{-6}$	1.006	0.801	0.658	0.553	0.475	1.008	0.805	0.663	0.560	0.483
$8.24\cdot10^{-6}$	1.010	0.805	0.661	0.556	0.478	1.012	0.808	0.666	0.563	0.486
$1.50\cdot10^{-5}$	1.012	0.807	0.662	0.557	0.479	1.014	0.810	0.667	0.563	0.487
$3.75\cdot10^{-5}$	1.024	0.816	0.670	0.563	0.483	1.025	0.819	0.674	0.569	0.491
$7.49\cdot10^{-5}$	1.044	0.831	0.682	0.573	0.491	1.043	0.833	0.685	0.578	0.498
$1.50\cdot10^{-4}$	1.084	0.862	0.707	0.593	0.508	1.080	0.862	0.709	0.597	0.514
$2.25\cdot10^{-4}$	1.085	0.863	0.708	0.594	0.509	1.079	0.861	0.708	0.597	0.514

[a]Standard uncertainties are $u(T)$ = 0.02 K, $u(P)$ = 10 kPa and $u_r(\eta)$ = 0.01 (0.95 level of confidence). [b]C is the volume concentration of C_{70}-Met and C_{70}-Cys in aqueous solution at P = 0.1 MPa.

$$r_{C_{70}-Cys} \approx R_{C_{70}-Cys}/M_{C_{70}-Cys} = 314.025/1203.48$$
$$\approx 0.2609 \pm 0.02 cm^3\cdot mol^{-1} (\approx 2.61\cdot10^{-4} m^3\cdot kg^{-1})$$

Thus, there is good agreement between the values calculated by using the Eisenlohr additivity rule and from the experimental data on the refraction indexes. When comparing the calculated and experimental values of the refractive indices with the literature data for water-soluble adducts of fullerenes C_{60}-Met[71] and C_{60}-Cys,[72] good agreement is seen.

3.2.3. Viscosity of Aqueous Solutions of C_{70}-Met and C_{70}-Cys. Table 5 and Figure S8 show T-x dependences of the dynamic viscosity (η) of C_{70}-Met and C_{70}-Cys at T = 293.15 to 333.15 K: the η increases with the rise of C_{70}-Met and C_{70}-Cys

https://doi.org/10.1021/acs.jced.5c00615
J. Chem. Eng. Data XXXX, XXX, XXX−XXX

concentration. The kinematic viscosities (η_k) were determined according to the following equation

$$\eta_k = \eta/\rho \tag{10}$$

where η is dynamic viscosity and ρ is the density of C_{70}-Met or C_{70}-Cys aqueous solutions.

The values of viscous flow activation ΔH^*, ΔS^*, and ΔG^* for C_{70}-Met and C_{70}-Cys aqueous solutions were calculated using Eyring transition state theory, according to the following eqs[40]

$$\Delta G^* = RT\ln\frac{\eta V}{hN_A} \tag{11}$$

$$\Delta H^* = -RT^2\frac{\partial}{\partial T}\left(\ln\frac{\eta V}{hN_A}\right) \tag{12}$$

$$\Delta S^* = -\frac{\Delta G^* - \Delta H^*}{T} \tag{13}$$

The activation energy of viscous flow (E_a), the entropic factor (A_s), and activation temperature (T_A) were determined using eqs 14, 15 (see Table S1)

$$\ln\eta = \ln A_S + \frac{E_a}{R}\frac{1}{T} \tag{14}$$

$$T_A = \frac{-E_a}{R\ln A_S} \tag{15}$$

Isoconcentrates of dynamic viscosity in the temperature range T = 293.15−333.15 K (Figures 2 and 3) were determined using the three-parameter Vogel−Fulcher−Tammann (VFT) equation (see Table S2)

$$\lg\eta(T) = \lg\eta_0 + A/(T - B) \tag{16}$$

where η_0, A, and B are adjustable parameters.

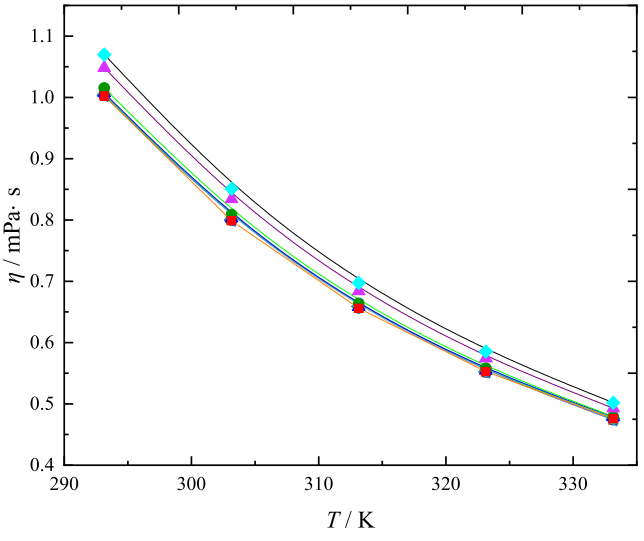

Figure 2. Temperature dependences (T) of the dynamic viscosity (η) of C_{70}-Met aqueous solutions at different concentrations ($x_{C_{60}-Met}$): (■) 0, (▲) 1.40·10^{-7}, (▼) 1.40·10^{-6}, (♦) 3.50·10^{-6}, (◀) 7.70·10^{-6}, (▶) 1.40·10^{-5}, (■) 3.50·10^{-5}, (●) 7.00·10^{-5}, (▲) 1.40·10^{-4}, (▼) 2.10·10^{-4}, (◆). Dots are experimental values; solid lines represent VFT equation approximation eq 16.

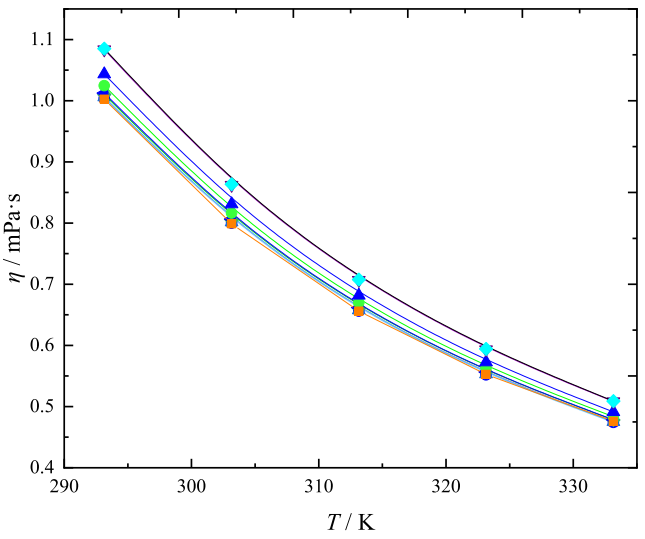

Figure 3. Temperature dependences of the dynamic viscosity (η) of C_{70}-Cys aqueous solutions at different concentrations ($x_{C_{60}-Cys}$): (■) 0, (▲) 1.50·10^{-7}, (▼) 1.50·10^{-6}, (♦) 3.75·10^{-6}, (◀) 8.24·10^{-6}, (▶) 1.50·10^{-5}, (■) 3.75·10^{-5}, (●) 7.49·10^{-5}, (▲) 1.50·10^{-4}, (▼) 2.25·10^{-4}, (◆). Dots are experimental values; solid lines represent VFT equation approximation eq 16.

The values of adjustable parameters for the VFT equation as well as AAD and SD values are presented in Table S2.

The present study of the viscosities of C_{70}-Met and C_{70}-Cys has shown the similarity of the behavior of aqueous solutions for such binary systems as C_{60}-Met−H_2O,[71] C_{60}-Cys−H_2O[72] $C_{60}[C(COOH)_2]_3$−H_2O,[57] $C_{60}(OH)_{22-24}$−H_2O, $C_{70}(OH)_{12}$−H_2O.[47,52]

3.2.4. Electrical Conductivity of Aqueous Solutions of C_{70}-Met and C_{70}-Cys. Eqs 17 and 18 were used to calculate specific (κ) and molar (Λ) electrical conductivities of C_{70}-Met and C_{70}-Cys aqueous solutions at 298.15 K

$$\kappa = \Lambda\cdot C_M \tag{17}$$

$$\Lambda = (1000\cdot\kappa)/C_M \tag{18}$$

where C_M is the molar concentration of the solution.

Table 6 presents the experimental data on concentration dependencies of κ and Λ at T = 298.15 K.

The analysis of obtained data shows an increase of specific electrical conductivity and a decrease of molar electrical conductivity with an increase of C_{70}-Met and C_{70}-Cys concentrations.

The molar electrical conductivity in infinitely dilute solutions (Λ_0) was calculated by the extrapolation of $\Lambda(\sqrt{C_M})$ to $\sqrt{C_M} = 0$ according to the Kohlrausch equation eq 19

$$\Lambda = \Lambda_0 - A\cdot\sqrt{C_M} \tag{19}$$

where A is an empirical value that depends on the nature of electrolyte and solvent, as well as temperature and pressure.

The degree of dissociation (α) and dissociation constant (K_D) of C_{70}-Met and C_{70}-Cys in aqueous solutions were determined using eqs 20 and 21, assuming a proton dissociation mechanism for C_{70}-Met ($C_{70}(C_4H_{10}NSCOOH)_3$ ⇄ $C_{70}(C_4H_{10}NSCOOH)_2C_4H_{10}NSCOO^- + H^+$) and C_{70}-Cys ($C_{70}(C_2H_6NSCOOH)_3$ ⇄ $C_{70}(C_2H_6NSCOOH)_2C_2H_6NSCOO- + H+$)

https://doi.org/10.1021/acs.jced.5c00615
J. Chem. Eng. Data XXXX, XXX, XXX−XXX

Table 6. Concentration Dependencies of Specific (κ) and Molar (Λ) Electrical Conductivities of C_{70}-Met and C_{70}-Cys Aqueous Solutions, as Well as Degree of Dissociation (α) and pK_D Values of Fullerene Adducts at T = 298.15 K[a]

x	κ/mS·cm^{-1}	Λ/S·m^2·mol^{-1}	α	pK_D
		C_{70}-Met		
0		0.67 ± 0.02*	1.000	3.72 ± 0.2*
$7\cdot10^{-7}$	0.023	0.582	0.874	3.63 ± 0.2
$1.40\cdot10^{-6}$	0.043	0.547	0.822	3.35 ± 0.2
$2.8\cdot10^{-6}$	0.077	0.495	0.743	3.48 ± 0.1
$7\cdot10^{-6}$	0.159	0.410	0.616	3.41 ± 0.1
$1.4\cdot10^{-5}$	0.264	0.339	0.509	3.39 ± 0.1
$2.1\cdot10^{-5}$	0.350	0.300	0.451	3.36 ± 0.1
$2.8\cdot10^{-5}$	0.431	0.277	0.416	3.34 ± 0.1
$3.5\cdot10^{-4}$	0.502	0.258	0.388	3.32 ± 0.2
		C70-Cys		
0		0.67 ± 0.02*	1.000	3.97 ± 0.2*
$7.49\cdot10^{-7}$	0.022	0.530	0.785	3.93 ± 0.2
$1.50\cdot10^{-6}$	0.039	0.469	0.696	3.88 ± 0.2
$3.0\cdot10^{-6}$	0.070	0.422	0.625	3.76 ± 0.1
$7.49\cdot10^{-6}$	0.135	0.326	0.483	3.73 ± 0.1
$1.50\cdot10^{-5}$	0.211	0.254	0.376	3.72 ± 0.1
$2.25\cdot10^{-5}$	0.273	0.219	0.325	3.71 ± 0.1
$3.0\cdot10^{-5}$	0.326	0.196	0.290	3.70 ± 0.1
$3.75\cdot10^{-4}$	0.376	0.181	0.268	3.69 ± 0.1

[a]Combined expanded uncertainty is $u_c(\kappa)$ = 0.01 mS·cm^{-1} for T = 298.15 K (0.95 level of confidence); *obtained by extrapolation.

$$\alpha = \Lambda/\Lambda_0 \quad (20)$$

$$K_D = \frac{C_M \cdot \alpha^2}{(1-\alpha)} \quad (21)$$

The calculated concentration dependences of α (Figure S9) and pK_D are presented in Table 6 and reveal that C_{70}-Met and C_{70}-Cys are weak electrolytes.

The degree of dissociation (α) increase upon dilution of the solution from ≈0.388 to 1.00 for C_{70}-Met and ≈0.268 to 1.00 for C_{70}-Cys is quite natural; it is observed for all aqueous solutions of electrolytes when determining the characteristics of dissociation by the electrical conductivity method. A similar tendency was observed for all previously studied adducts of light fullerenes with amino acids.[42,73,74] This fact is because the electrophoretic and relaxation effects increase with the concentration of the electrolyte, leading to decreases in the charge transfer and the mobility of ions. In principle, the decrease in the strength of the electrolyte with an increasing concentration in highly polar solvents (water) is a well-known fact. It should also be noted that the obtained values of the molar conductivity in infinitely dilute solutions ($\Lambda_\circ$ (C_{70}-Met) ≈ 0.67 ± 0.02 S·m^2·mol^{-1} and $\Lambda_\circ$ (C_{70}-Cys) ≈ 0.67 ± 0.02 S·m^2·mol^{-1}) are in agreement with triple molar conductivity of a proton in aqueous solutions ($\Lambda_\circ$ = 0.225·3 = 0.675 S·m^2·mol^{-1}).[75] This fact allows us to suggest that the dissociation of C_{70}-Met and C_{70}-Cys in infinitely dilute solutions is accompanied by the release of three hydrated protons.

The thermodynamic dissociation constant (K_D^{therm}) was calculated by extrapolating the K_D values to the region of an infinitely dilute solution

$$K_D^{therm} = \lim_{C_M \to 0} K_D \quad (22)$$

The pK_D^{therm} value for C_{70}-Met is equal to 3.72 and for C_{70}-Cys it is 3.97, while the pK_D value of the carboxyl group in L-Met is equal to 2.13 and 1.89 for L-Cys.[76] According to the classical Lewis acid−base theory, electron-donating substituents reduce the strength of acids and increase the strength of bases, and conversely, electron-withdrawing substituents increase the strength of acids and reduce the strength of bases. Thus, attaching an amino acid to the C_{70} core leads to a decrease in the acidity of the carboxyl group. The obtained result is consistent with the fact that fullerenes can exhibit electron-donor properties.[77]

Considering that aqueous solutions of C_{70}-Met and C_{70}-Cys form associates, the K_D values are conditional. A monotonic decrease of pK_D (from ≈3.72 to 3.32 for C_{70}-Met and ≈3.97 to 3.69 for C_{70}-Cys) with increasing concentration is quite difficult to explain (see Table 6). The calculation of pK_D was carried out using Ostwald's dilution law eq 22, without taking into account the activity coefficients of ion-molecular forms. Moreover, the charge carriers in the system under study change depending on concentration: monomeric forms (which were not detected in the studied concentration range), associates of the first, second, and third orders (Table 6). The activity coefficients of the monomers inside such associates are not available, but from general considerations in strongly associated concentrated solutions of electrolytes large (sometimes extreme) positive deviations from ideality are observed using asymmetric normalization of excess functions. For example, in concentrated aqueous solutions of $(UO_2)Cl_2$ the values of the average ionic activity coefficients are $\gamma^{\pm} \approx$ 2000÷3000 rel. units.[78] Taking into account the activity coefficients of globally associated C_{70}-Met and C_{70}-Cys should significantly reduce the values of thermodynamic dissociation constants with increasing concentration and make the calculation correct.

3.2.5. Surface Properties of C_{70}-Met and C_{70}-Cys Water Solutions. Plate mass values based on electronic microbalance readings were used to calculate the surface tension of C_{70}-Met and C_{70}-Cys aqueous solutions eq 23

$$\gamma = mk \quad (23)$$

where m is the mass of the plate, $k = \gamma(H_2O)/m$ is a constant depending on the characteristics of the plate, the value of which was found from calibration experiments with water. Figure S10 presents the kinetic dependencies of γ at different concentrations of C_{70}-Met and C_{70}-Cys aqueous solutions. The obtained data shows that (i) surface tension of C_{70}-Met and C_{70}-Cys aqueous solutions depends on concentration, (ii) C_{70}-Met−H_2O and C_{70}-Cys−H_2O systems need about 20 to 500 min to reach equilibria, depending on the concentrations of C_{70}-Met and C_{70}-Cys in solution (Figure S10). Figure 4 presents the surface tension isotherms for C_{70}-Met and C_{70}-Cys aqueous solution at T = 298.15−313.15 K.

As can be seen, C_{70}-Met reduces the γ value down to 56.84 mN·m^{-1} at $x_{C_{70}-Met} = 2.80\cdot10^{-4}$ and C_{70}-Cys to 57.84 mN·m^{-1} at $x_{C_{70}-Cys} = 3.00\cdot10^{-4}$ (at 298.15 K). The surface tension of C_{70}-Met and C_{70}-Cys solutions significantly depends on the concentration.

For the investigation of the surface morphology in C_{70}-Met−H_2O and C_{70}-Cys−H_2O binary systems, adsorption films were obtained and studied by using AFM.

The adsorption films of C_{70}-Cys (*a*, $x = 7.49\cdot10^{-6}$; *b*, $x = 7.49\cdot10^{-5}$) and C_{70}-Met (*c*, $x = 7.0\cdot10^{-6}$; *d*, $x = 7.0\cdot10^{-5}$)

https://doi.org/10.1021/acs.jced.5c00615
J. Chem. Eng. Data XXXX, XXX, XXX−XXX

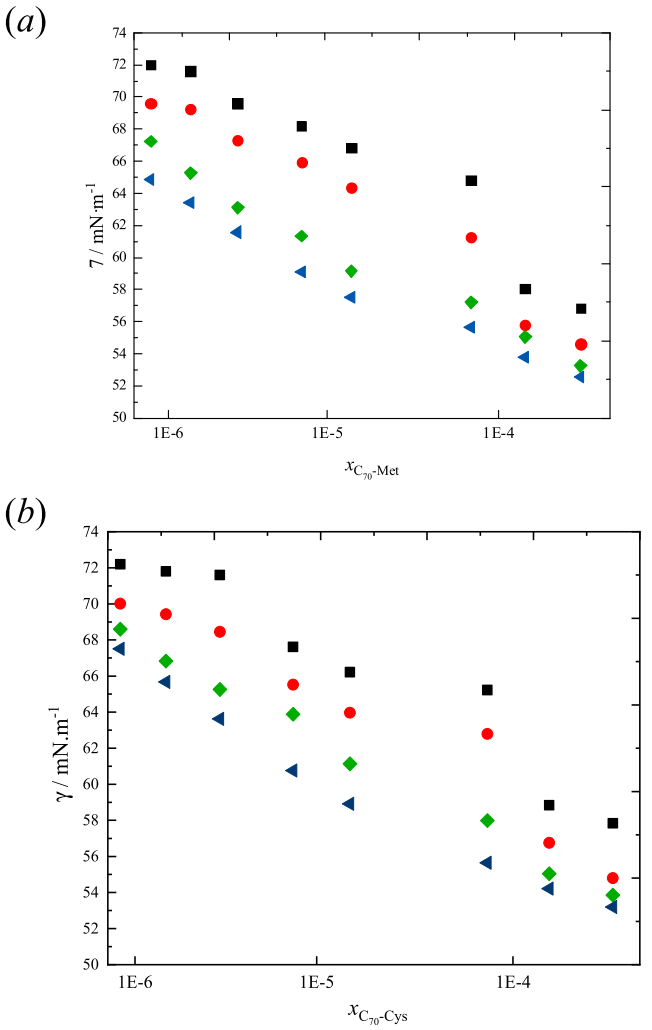

Figure 4. Surface tension (γ) of C_{70}-Met (*a*) and C_{70}-Cys (*b*) aqueous solutions at T = (■) 298.15 κ; (●) 303.15 κ; (♦) 308.15 κ and (◀) 313.15 κ in the concentration range $x_i = 7.70 \cdot 10^{-7} - 3.00 \cdot 10^{-4}$; x_i is a mole fraction of C_{70}-Met or C_{70}-Cys.

aqueous solutions were transferred to a freshly formed mica surface and studied using atomic force microscopy (Figure 5).

AFM images of C_{70}-Cys and C_{70}-Met show that the surface layers contain associates (Table 9 and Figure S11). The solutions of C_{70}-Cys with concentration $x = 7.49 \cdot 10^{-6}$ (Figure 5a) are characterized by the presence of associates with sizes of the order of several tens of nanometers. A 10-fold increase in the concentration leads to the appearance of much larger associates in the solution, from several hundred nanometers to about 1−2 μm (Figure 5b). The presence of particles with the diameter less than 100 nm remains in the solution, which may not be detected in the DLS results due to the fact that large particles mainly scatter light in this case. For C_{70}-Met solution with concentration $x = 7.0 \cdot 10^{-6}$ (Figure 5c), the presence of associates with sizes from several tens to hundreds of nanometers was detected which also confirms the results of DLS. An increase in the concentration of C_{70}-Met (Figure 5d), as in the case of C_{70}-Cys solutions, leads to the appearance of micrometer size particles in the solution.

3.2.6. Solubility of C_{70}-Met and C_{70}-Cys in Water. The solubility in binary systems C_{70}-Met−H_2O and C_{70}-Cys−H_2O in the temperature range T = 298.15 to 333.15 K is presented in Figure 6, from which it follows that (i) the solubility curve contains one branch; an increase in solubility with raising temperature is observed, (ii) the equilibrium solid phases in the whole temperature range are crystal hydrates C_{70}-Met·$4H_2O$ and C_{70}-Cys·$4H_2O$, (iii) C_{70}-Met and C_{70}-Cys are compatible with water and according to Figure 6 their solubility varies from ω = 0.012 to 0.061 for C_{70}-Met and ω = 0.010 to 0.052 for C_{70}-Cys. For the comparison, the solubility values at 298.15 K for the following binary systems are C_{60}-Arg-H_2O (ω = 0.019),[18] C_{60}-Thr-H_2O (ω = 0.0412),[43] C_{60}-Lys-H_2O (ω = 0.0253).[79]

Determining the solubility in the ternary C_{70}-Met−NaCl−H_2O and C_{70}-Cys−NaCl−H_2O systems is important for further biomedical applications of C_{70}-Met and C_{70}-Cys. Figure 7 shows that the solubility diagrams consist of two branches corresponding to the crystallization of the crystal hydrates of the composition C_{70}-Met·$4H_2O$ or C_{70}-Cys·$4H_2O$ and NaCl. The diagrams consist of one invariant point (point E), which corresponds to the simultaneous saturation by the C_{70}-Met·$4H_2O$ or C_{70}-Cys·$4H_2O$ and NaCl solid phases.

3.2.7. Distribution of C_{70}-Met and C_{70}-Cys in the *n*-Octanol−Water Systems. The value of $\lg P_{ow}$ for C_{70}-Met is equal to −0.914 and that for C_{70}-Cys is −0.956. The obtained values indicate that C_{70}-Met and C_{70}-Cys have similar affinity to the aqueous and *n*-octan-1-ol phases. It is well-known that in the case of $\lg P_{ow} = -1 \div 2$ the biological active substances are suitable for oral administration. At a low value of $\lg P_{ow} < -1$ the biological active substance is poorly absorbed and, finally, at $\lg P_{ow} > 2$ the substance will be retained in the lipid bilayer.[80]

3.2.8. Cryoscopy of C_{70}-Met and C_{70}-Cys. The experimental values of decreasing the ice crystallization temperature for the C_{70}-Met−H_2O and C_{70}-Cys−H_2O binary systems are presented in Figure 8 and Table 7. The results show that the obtained dependences are extremely nonlinear (the curves are concave) in the entire concentration range, even for diluted solutions. For comparison, the concentration dependence of ice crystallization temperatures for ideal solutions is shown in Figure 8. It can be seen that the obtained values of the decrease in ice crystallization temperatures for C_{70}-Met and C_{70}-Cys aqueous solutions are significantly higher than the corresponding decrease for the ideal solutions. This fact indicates positive deviations from ideality for the C_{70}-Met and C_{70}-Cys solutions. To calculate the water activity values eq 24 was applied[81]

$$\ln a_w = \frac{-\Delta H_w{}^f \Delta T - \Delta C_p \Delta T^2}{R \cdot (T_0^f - \Delta T) T_0^f} \quad (24)$$

where $\Delta H_{H_2O}{}^f$ is the melting enthalpy of ice (5990 J·mol^{-1}); ΔC_P is the change of isobaric heat capacity for the ice melting process (−38.893 J·mol^{-1}·K^{-1}); T^f_0 = 273.15 K is the ice melting point; a_{H2O} is activity of water; $\Delta T = T^f_0 - T$, T is the temperature of the beginning of crystallization process in C_{70}-Met (or C_{70}-Cys) aqueous solutions; R is the universal gas constant.

To calculate the activity coefficients of the fullerene adducts in the binary systems C_{70}-Met−H_2O and C_{70}-Cys−H_2O, the VD-AS model was used, which is based on the virial decomposition of the excess molar Gibbs energy in mole fractions of the solution components. This approach has been used previously for thermodynamic description of binary systems, containing fullerene adducts $C_{60}(OH)_{24}$−H_2O,[47] $C_{70}(C_6H_{14}N_2O_2)_3$−$H_2O$,[45] $C_{60}[(C(COOH)_2]_3$−H_2O,[82]

https://doi.org/10.1021/acs.jced.5c00615
J. Chem. Eng. Data XXXX, XXX, XXX−XXX

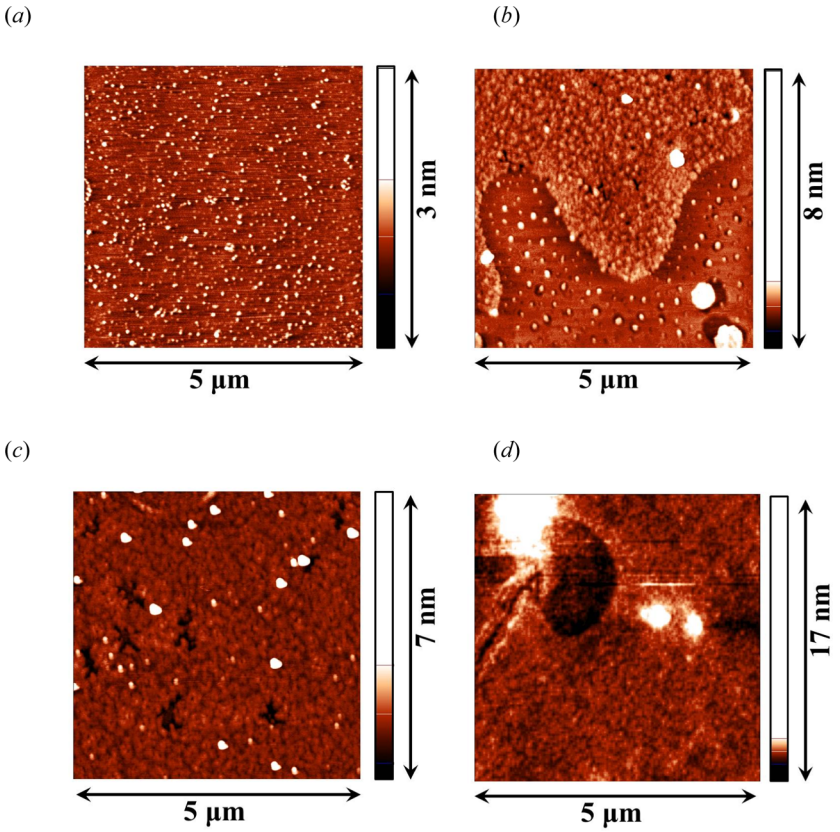

Figure 5. AFM images of C_{70}-Cys (a, $x = 7.49 \cdot 10^{-6}$; b, $x = 7.49 \cdot 10^{-5}$) and C_{70}-Met (c, $x = 7.0 \cdot 10^{-6}$; d, $x = 7.0 \cdot 10^{-5}$) adsorbed films; components applied onto the mica surface as droplets (transferred from the water surface to the mica surface by the Langmuir-Schaeffer method).

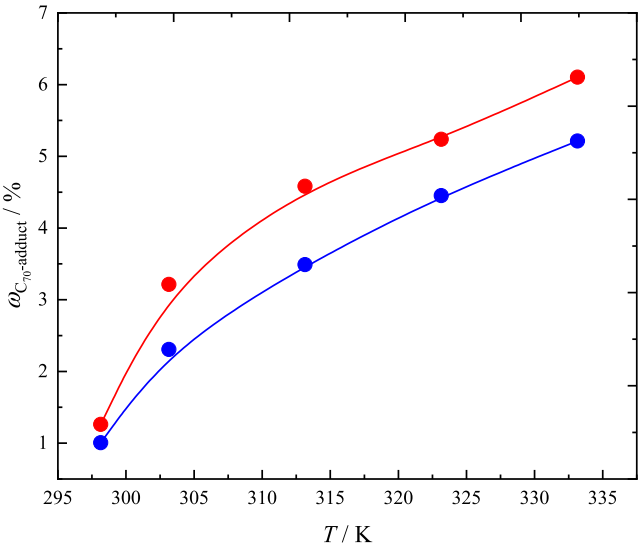

Figure 6. Solubility in the binary systems C_{70}-Met–H_2O (red line) and C_{70}-Cys–H_2O (blue line) at 298.15 to 333.15 K. ω is the mass fraction of C_{70}-Met or C_{70}-Cys and T is the absolute temperature (black dots are experimental data).

$C_{70}(OH)_{12}-H_2O$, $C_{70}[C(COOH)_2]_3-H_2O$, $C_{60}(C_5H_9NO_3)_2-H_2O$, $C_{60}(C_6H_{14}N_2O_2)_2-H_2O$,[81] $C_{70}(C_4H_9NO_2)_2-H_2O$.[46] According to semiempirical VD-AS model the following expression can be assumed (index 1 is referred to C_{70}-Met or C_{70}-Cys) and index 2 to H_2O)[83]

$$\frac{G^E}{RT} = (n_1 + n_2) \sum_{=1} \sum_{j=1} x_1^i x_2^j \cdot \lambda_{ij} = \frac{\sum_{=1} \sum_{j=1} x_1^i x_2^j \cdot \lambda_{ij}}{(n_1 + n_2)^{i+j-1}} \quad (25)$$

where G^E is the total molar excess Gibbs energy of the solution, T is the absolute temperature, n_k and x_k are the mole number and mole fraction of the k-th component, λ_{ij} is an ij–virial coefficient in the expansion of $\frac{G^E}{RT}$ according to the mole numbers of the components. On the basis of the VD-AS model we obtained the following equations for calculation of activity coefficients in "asymmetric" type of normalization[81]

$$\ln \gamma_1^{ass} \approx 2\Lambda_2 x_1 + 3\Lambda_3 x_1^2 + 4\Lambda_4 x_1^3 \quad (26)$$

$$\ln \gamma_2^{ass} \approx -\Lambda_2 x_1^2 - 2\Lambda_3 x_1^3 - 3\Lambda_4 x_1^4 \quad (27)$$

where $\Lambda_i(T) = \sum_{=1} \lambda_{ij}$.

From the obtained $\ln\gamma_2(x_1)$ dependencies the model parameters (Λ_2, Λ_3, Λ_4) were calculated (see Table 8). The calculated concentration dependences of C_{70}-Met and C_{70}-Cys activity coefficients are presented in Table 8 and Figures 9 and 10.

According to eq 28 the concentrations corresponding to thermodynamic stability loss were determined

$$F(x_1) = \frac{\partial^2 \left(\frac{G^{mix}}{RT}\right)}{\partial x_1^2} = 12\Lambda_4 x_1^3 + 6\Lambda_3 x_1^2 + 2\Lambda_2 x_1 + 1 = 0 \quad (28)$$

https://doi.org/10.1021/acs.jced.5c00615
J. Chem. Eng. Data XXXX, XXX, XXX–XXX

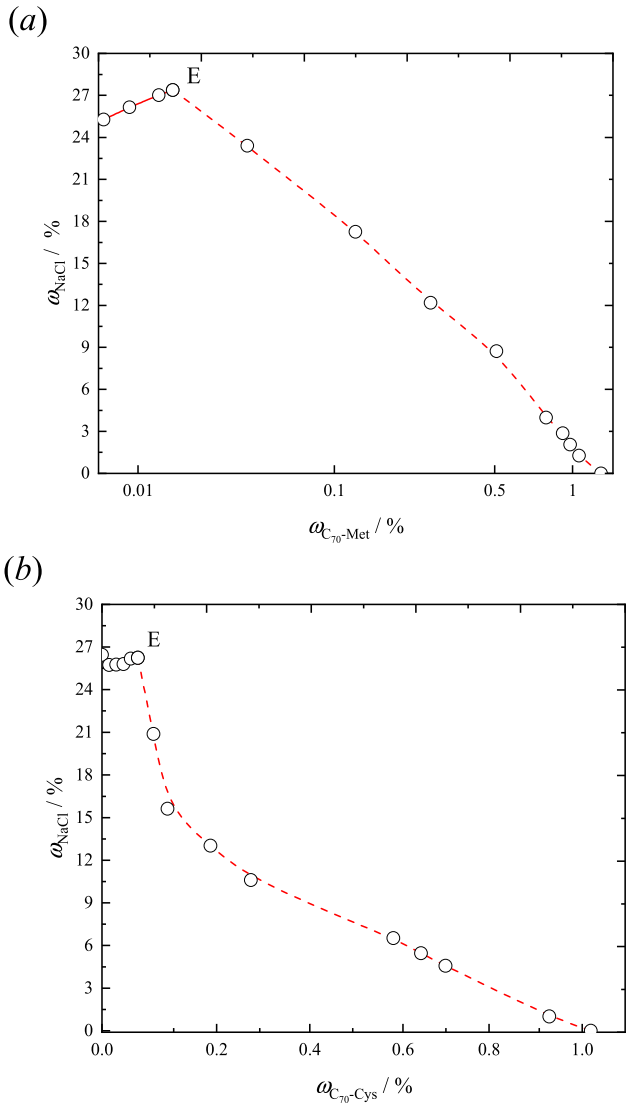

Figure 7. Solubility in C_{70}-Met−NaCl−H_2O (a) and C_{70}-Cys−NaCl−H_2O (b) ternary systems at 298.15 K (the dashed line corresponds to the crystallization of the C_{70}-adduct·4H_2O; the solid line corresponds to the crystallization of NaCl); ω is the mass fraction and E is a invariant point which corresponds to the saturation by C_{70}-Met·4H_2O + NaCl (Figure 7a) or C_{70}-Cys·4H_2O + NaCl (Figure 7b).

The obtained concentrations corresponding to the loss of thermodynamic stability by aqueous solutions were compared with experimental data on nanoparticles size distribution in C_{70}-Met−H_2O and C_{70}-Cys−H_2O binary systems (Table 9 and Figure S11). Table 9 and Figure S11 reveal the following: (i) there are no C_{70}-Met and C_{70}-Cys monomeric molecules in the aqueous solution in the concentration range $x = 1.4\cdot10^{-8}$–$7.0\cdot10^{-5}$ for C_{70}-Met and $x = 1.5\cdot10^{-8}$–$7.49\cdot10^{-5}$ for C_{70}-Cys; (ii) in the range of low concentrations (up to $x = 7.0\cdot10^{-6}$ for C_{70}-Met and $x = 3.75\cdot10^{-6}$ for C_{70}-Cys), the solutions contain first-order associates 30−50 nm in size; (iii) second-order associates of 100−400 nm were detected in the concentration range $x = 3.5\cdot10^{-6}$–$7.0\cdot10^{-5}$ for C_{70}-Met and $x = 3.75\cdot10^{-6}$–$7.49\cdot10^{-5}$ for C_{70}-Cys; (*iv*) in more concentrated solutions (up to $x = 7.0\cdot10^{-5}$ for C_{70}-Met and $x = 7.49\cdot10^{-5}$ for C_{70}-Cys) the simultaneous presence of second- and third-order associates of 1−2 μm in size were detected in both systems. Additionally, the concentration dependences of the ζ potential for the C_{70}-Met and C_{70}-Cys aqueous solutions are presented in Table 9. The data reveals the following: (i) ζ potential values are negative (in the concentration range $x = 1.4\cdot10^{-8}$–$7.0\cdot10^{-5}$ for C_{70}-Met and $x = 1.5\cdot10^{-8}$–$7.49\cdot10^{-5}$ for C_{70}-Cys); (ii) aqueous dispersions of C_{70}-Cys and C_{70}-Met possess aggregative stability over the whole concentration range; (iii) the C_{70}-Cys and C_{70}-Met aqueous solutions are highly

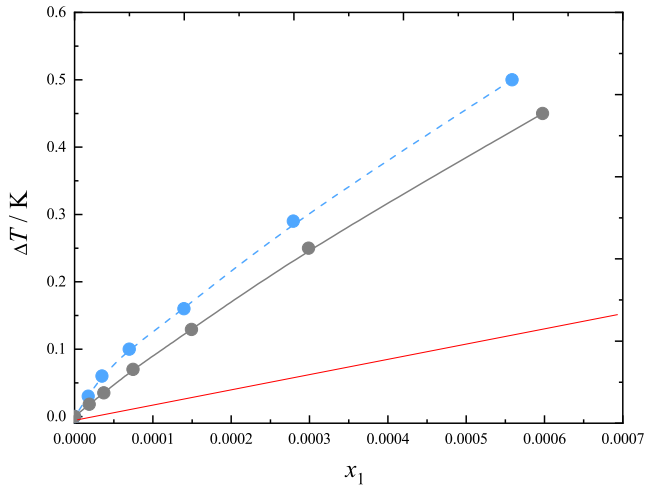

Figure 8. Concentration dependence of ice crystallization temperature for the binary systems: C_{70}-Met−H_2O (dashed blue line) and C_{70}-Cys−H_2O (solid gray line) in the temperature range T = 272.15–273.15 K. The red line corresponds to the ideal nonelectrolyte aqueous solution. x_1 is the molar fraction of C_{70}-Met or C_{70}-Cys and ΔT is the ice crystallization temperature.

Table 7. Cryometric Investigation of C_{70}-Met−H_2O and C_{70}-Cys−H_2O Binary Systems[a,b]

		C_{70}-Met−H_2O			C_{70}-Cys−H_2O		
C/g·dm^{-3}	ΔT/K	x_1	lnγ_2	lnγ_1^{ass}	x_1	lnγ_2	lnγ_1^{ass}
1.25	0.07	$1.75\cdot10^{-5}$	$-2.90\cdot10^{-4}$	$-2.72\cdot10^{-4}$	$1.86\cdot10^{-5}$	$-1.73\cdot10^{-4}$	$-1.55\cdot10^{-4}$
2.50	0.13	$3.49\cdot10^{-5}$	$-5.80\cdot10^{-4}$	$-5.45\cdot10^{-4}$	$3.73\cdot10^{-5}$	$-3.38\cdot10^{-4}$	$-3.0\cdot10^{-4}$
5.00	0.24	$6.99\cdot10^{-5}$	$-9.67\cdot10^{-4}$	$-8.97\cdot10^{-4}$	$7.46\cdot10^{-5}$	-6.76×10^{-4}	$-6.02\cdot10^{-4}$
10.00	0.31	$1.40\cdot10^{-4}$	$-1.55\cdot10^{-3}$	$-1.41\cdot10^{-3}$	$1.49\cdot10^{-4}$	$-1.25\cdot10^{-3}$	$-1.10\cdot10^{-3}$
20.00	0.38	$2.79\cdot10^{-4}$	$-2.81\cdot10^{-3}$	$-2.53\cdot10^{-3}$	$2.98\cdot10^{-4}$	$-2.42\cdot10^{-3}$	$-2.12\cdot10^{-3}$
40.00	0.50	$5.59\cdot10^{-4}$	$-4.86\cdot10^{-3}$	$-4.30\cdot10^{-3}$	$5.97\cdot10^{-4}$	$-4.37\cdot10^{-3}$	$-3.77\cdot10^{-3}$

[a]Standard uncertainty is $u(\Delta T)$ = 0.005÷0.01 K at the used resolution of a Beckman thermometer at ~0.005 K/1 mm (0.95 level of confidence). [b]C is the molar concentration; ΔT is the ice crystallization temperature; x_1 is the molar fraction of C_{70}-Met or C_{70}-Cys; lnγ_2 is the logarithm of water activity coefficient; lnγ_1 the logarithm of C_{70}-Met and C_{70}-Cys activity coefficient.

Table 8. VD-AS Model Parameters (Λ_2, Λ_3, Λ_4) and Concentration Range of Thermodynamic Stability ($X^{diff\text{-}instab}$) for the Binary Systems C_{70}-Met−H_2O and C_{70}-Cys−H_2O

	VD-AS parameters				
	Λ_2	Λ_3	Λ_4	R^2	$x^{diff\text{-}instab}$
C_{70}-Met	$1.61\cdot10^5$	$-3.28\cdot10^8$	$2.35\cdot10^{11}$	0.976	$2.72\cdot10^{-4}$
C_{70}-Cys	$1.01\cdot10^5$	$-1.83\cdot10^8$	$1.20\cdot10^{11}$	0.992	$3.29\cdot10^{-4}$

https://doi.org/10.1021/acs.jced.5c00615
J. Chem. Eng. Data XXXX, XXX, XXX−XXX

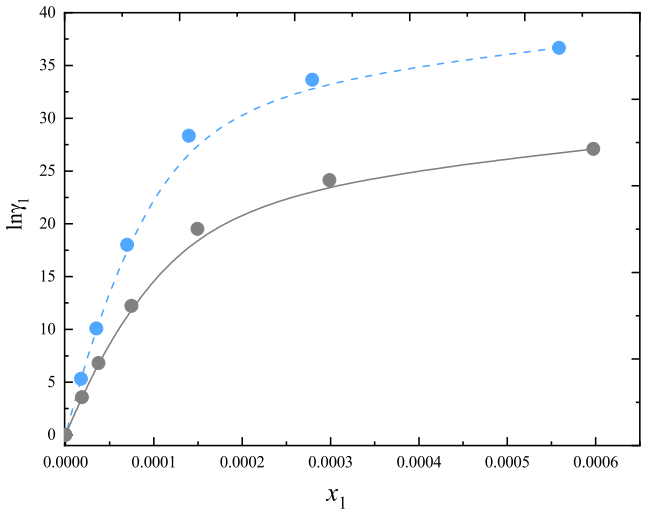

Figure 9. Concentration dependences of the logarithm of the C_{70}-Met and C_{70}-Cys activity coefficient ($\ln\gamma_1$) in the binary systems. C_{70}-Met−H_2O (dashed blue line) and C_{70}-Cys−H_2O (solid gray line). x_1 is the molar fraction of C_{70}-Met and C_{70}-Cys.

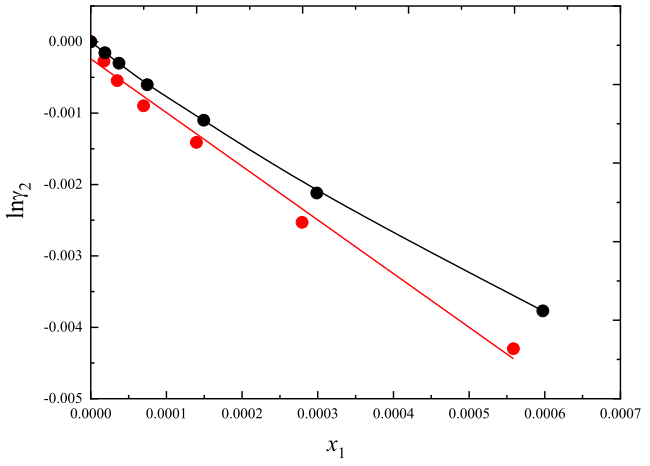

Figure 10. Concentration dependences of the logarithm of the water activity coefficient ($\ln\gamma_2$) in the binary system: C_{70}-Met−H_2O (red line) and C_{70}-Cys−H_2O (black line). x_1 is molar fraction of C_{70}-Met and C_{70}-Cys in the aqueous solution.

associated and there are no adequate equations for calculating of ζ-potential, thus the ζ-potential values obtained according to Helmholtz-Smoluchowski equation are approximate and can be used only for the crude estimation of the surface charge density of the species.[84]

f11 According to Figure 11, we can conclude that at concentrations less than $x_1^{\text{diff-instab}} = 2.72\cdot10^{-4}$ for C_{70}-Met and $x_1^{\text{diff-instab}} = 3.29\cdot10^{-4}$ for C_{70}-Cys the C_{60}-Cys−H_2O and C_{60}-Met−H_2O systems are stable (no phase separation takes place) and when $x_1^{\text{diff-instab}} = 2.72\cdot10^{-4}$ for C_{70}-Met and $x_1^{\text{diff-instab}} = 3.29\cdot10^{-5}$ for C_{70}-Cys the miscibility of solutions starts. Finally, when $x_1 > x_1^{\text{diff-instab}}$ the solutions lose the diffusion stability (the miscibility of solution takes place).

3.2.9. Correlation between Physicochemical Properties. For the description of $T-x$ dependencies of refraction indexes, viscosity, density, and electrical conductivity the following equation was applied

$$P = a + \sum_{i=1}^{4} b_i \cdot T^i + \sum_{j=1}^{4} c_j \cdot C^j \quad (29)$$

where P is a value of the physical property (refraction indexes, viscosity, density, and electrical conductivity), a, b_i, c_j are the correlation parameters (see Table S3). The comparison of the experimental and calculated data is presented in Figures 12 and f12f13 13. f13

3.3. Computer Simulations

Since the C_{70} molecule contains five types of nonequivalent carbon atoms, taking into account that three amino acid residues L-Met or L-Cys are attached to the fullerene core, it is important to determine the most stable isomer. To understand this, the electronic structures (Table 10), HOMO and LUMO, t10 as well as the total energies of the isomers were calculated. The calculation of the electronic structures showed that in both cases the most favorable structures are the isomers with the Saturn-like arrangement of substituents on the almost-terminal part of the fullerene core (isomer #4, Table 10).

The isomers of C_{70}-Met and C_{70}-Cys with a Saturn-like distribution of residues on the almost terminal part of the fullerene core were chosen for computer modeling. Radial distribution functions between specific C_{70}-Met and C_{70}-Cys atoms and water calculated using the MD method were obtained to identify the distances at which water molecules approach the atoms of the fullerene adducts in the aqueous solution (Figure 14). f14

As can be seen from the obtained data: (i) water molecules are closer to the carboxyl group of C_{70}-Met or C_{70}-Cys and (ii) the number of water molecules localized at nitrogen atoms is noticeably smaller due to spatial hindrances caused by the fullerene core and amino acid residue. However, in the case of C_{70}-Met, the presence of water molecules is observed near the carbon atom connected to the nitrogen atom by a covalent bond, while in C_{70}-Cys, this area is shielded from water molecules.

Visualization of the system configurations shows a weak interaction of C_{70}-Met molecules with each other. To establish the nature of the interaction between fullerene adducts during associate formation, $10C_{70}$-Cys or C_{70}-Meth molecules were uniformly distributed randomly among 2000 water molecules. This system was modeled in the *NPT* ensemble at 298 K. It is seen that at the beginning of modeling, the adduct molecules were uniformly distributed in the volume of water. Results of modeling showed that the formation of associates for both adducts occurs through a fullerene core contact. Thus, hydrophobic interactions play a crucial role in the formation of associate. As an example, Figure 15 shows the results of f15 association process modeling binary C_{70}-Met−H_2O system.

As can be seen, after 1 ns from the beginning of modeling, the molecules combined into dimers (Figure 15c).

3.4. Biocompatibility Study

3.4.1. Antiradical Activity (DPPH). The mechanism of interaction of C_{70} adducts with DPPH is proposed in Figure S12 and includes two stages: the transfer of a hydrogen ion to the radical (fast stage) and the nucleophilic attack of the radical on the π-bond of the fullerene core (slow stage).

To quantitatively estimate the reaction rate between C_{70}-Met, C_{70}-Cys, and DPPH, a two-stage kinetic model of the pseudo-first-order reaction was used[66]

https://doi.org/10.1021/acs.jced.5c00615
J. Chem. Eng. Data XXXX, XXX, XXX−XXX

Table 9. Sizes of C_{70}-Met and C_{70}-Cys Associates in Aqueous Solutions at 298.15 K[a,b]

	x	δ_0/nm	δ_I/nm	δ_{II}/nm	δ_{III}/μm	$N_{0\rightarrow1}$	$N_{0\rightarrow2}$	$N_{0\rightarrow3}$	ζ_I, mV	ζ_{II}, mV	ζ_{III}, mV
						C_{70}-Met					
$x < x^{diff\text{-}instab}$	$1.4\cdot10^{-8}$		30−50			2×10^3−8×10^3			−41		
	$1.4\cdot10^{-7}$		30−50			2×10^3−8×10^3			−32		
	$3.5\cdot10^{-6}$		30−50	100−400		2×10^3−8×10^3	6.5×10^4−4.2×10^6		−33	−31	
	$7.0\cdot10^{-6}$		30−50	100−400		2×10^3−8×10^3	6.5×10^4−4.2×10^6		−37	−38	
	$1.05\cdot10^{-5}$			100−400			6.5×10^4−4.2×10^6			−38	
	$1.75\cdot10^{-5}$			100−400	1−2		6.5×10^4−4.2×10^6	6.5×10^7−5.2×10^8		−39	−47
$x > x^{diff\text{-}instab}$	$4.20\cdot10^{-5}$			100−400	1−2		6.5×10^4−4.2×10^6	6.5×10^7−5.2×10^8		−31	−52
	$7.0\cdot10^{-5}$			100−400	1−2		6.5×10^4−4.2×10^6	6.5×10^7−5.2×10^8		−36	−49
						C70-Cys					
$x < x^{diff\text{-}instab}$	$1.5\cdot10^{-8}$		30−50			2×10^3−8×10^3			−37		
	$1.5\cdot10^{-7}$		30−50			2×10^3−8×10^3			−33		
	$3.75\cdot10^{-6}$		30−50	100−400		2×10^3−8×10^3	6.5×10^4−4.2×10^6		−32	−39	
	$7.49\cdot10^{-6}$			100−400			6.5×10^4−4.2×10^6			−39	
	$1.12\cdot10^{-5}$			100−400			6.5×10^4−4.2×10^6			−40	
	$1.87\cdot10^{-5}$			100−400	1−2		6.5×10^4−4.2×10^6	6.5×10^7−5.2×10^8		−38	−55
$x > x^{diff\text{-}instab}$	$4.49\cdot10^{-5}$			100−400	1−2		6.5×10^4−4.2×10^6	6.5×10^7−5.2×10^8		−36	−54
	$7.49\cdot10^{-5}$			100−400	1−2		6.5×10^4−4.2×10^6	6.5×10^7−5.2×10^8		−33	−50

[a] $N_{0\rightarrow i}=\left(\frac{\delta_i}{\delta_0}\right)^3\cdot K_{pack}$, K_{pack} is the packing coefficient in the case of "small spheres packed into a large one" or, equivalently, the packing factor of a sphere into an equidimensional cube: $K_{pack}=\pi/6\approx0.52$. [b] x is the mole fraction of C_{70}-Met or C_{70}-Cys; δ_0, δ_i are average diameters of monomeric molecules and associates of the i-th order; $N_{0\rightarrow i}$ number of monomeric molecules in an i-th order associate; ζ_i is ζ-potential of the i-th order associates.

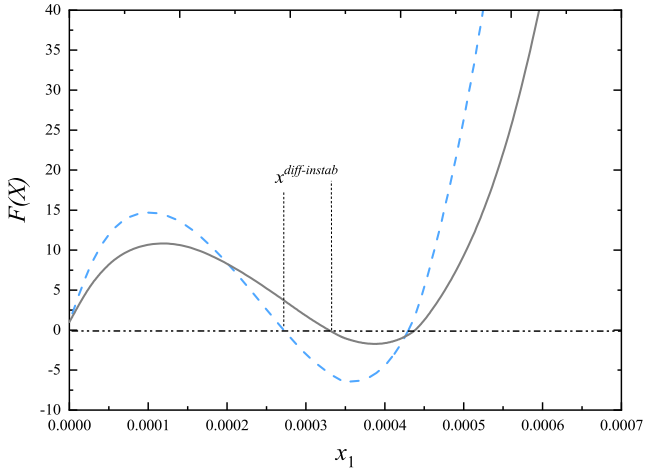

Figure 11. Concentration dependences of function $F(x_1)=12\Lambda_4x_1^3+6\Lambda_3x_1^2+2\Lambda_2x_1+1$ in the binary systems C_{70}-Met−H_2O (blue dashed line) and C_{70}-Cys−H_2O (gray solid line). x_1 is the molar fraction of C_{70}-Met or C_{70}-Cys in the aqueous solution.

$$\ln\frac{A_\infty-A_t}{A_\infty-A_0}=-kt \quad (30)$$

where A_∞, A_t, and A_0 are the optical densities of the solution at "infinity" (6 days after the start of the experiment), at time t, and at the initial time, respectively.

Figure S13 presents kinetic dependence of the reaction of DPPH reduction by the C_{70} adducts in the temperature range 298.15−318.15 K; from the slopes of the two sections of the kinetic curves, the values of the apparent rate constants at different temperatures were obtained (Table 11). Table 11 summarizes the rate constants obtained for various fullerene adducts with L-amino acids. The data reveal that experimental values are close to those obtained for such light fullerene adducts as C_{60} with L-Hyp ($C_{60}(C_5H_9NO_3)_2$), C_{60} with L-Arg ($C_{60}(C_6H_{13}N_4O_2)_8H_8$), C_{60} with Gly ($C_{60}(C_2NH_4O_2)_4H_4$), and C_{70} with L-Thr ($C_{70}(C_4H_9NO_3)_2$).

3.4.2. Interaction with DNA. Figure S14 shows the absorption spectra of DNA with the concentration of 6.49×10^{-8}−3.34×10^{-7} M in the presence of 6.49×10^{-8} M C_{70}-Met or C_{70}-Cys adducts. The hyperchromism can be explained by the presence of the following synergistic noncovalent interactions: external contact of C_{70}-Met and C_{70}-Cys and the sugar−phosphate backbone of the DNA molecule due to electrostatic interaction and formation of hydrogen bonds. Since there are no changes in the position of the absorption bands (bathochromic or hypochromic shifts), it can be

https://doi.org/10.1021/acs.jced.5c00615
J. Chem. Eng. Data XXXX, XXX, XXX−XXX

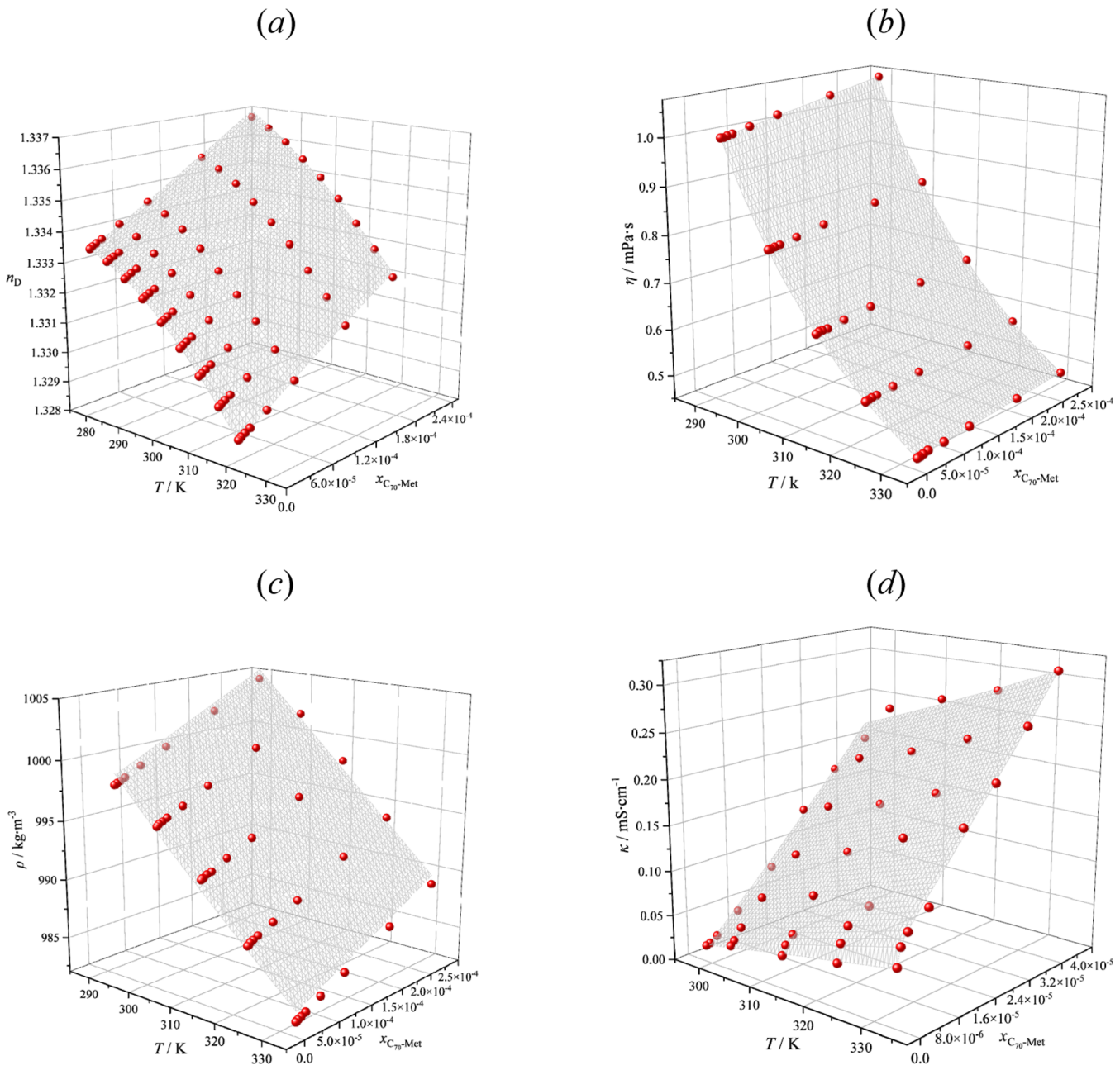

Figure 12. *T-C* dependences of refraction indices (*a*), viscosities (*b*), densities (*c*), and electrical conductivities (*d*) of C_{70}-Met aqueous solutions; red spheres are experimental data, surfaces are calculated data.

concluded that binding of C_{70}-Met and C_{70}-Cys to the grooves of the DNA molecule takes place.

The binding constant (K_b) was calculated using the Wolfe-Shimmer equation

$$\frac{[\mathrm{DNA}]}{\varepsilon_a - \varepsilon_f} = \frac{[\mathrm{DNA}]}{\varepsilon_b - \varepsilon_f} + \frac{1}{K_b(\varepsilon_b - \varepsilon_f)} \quad (31)$$

where [DNA] is the DNA concentration, ε_a, ε_f, ε_b are the extinction coefficients of the ligand complex with DNA, the ligand, and the ligand bound to DNA in stoichiometric amounts, respectively.

From the Wolfe−Shimmer dependences (in coordinates [DNA]/(ε_a−ε_f) on the [DNA] concentration) for the binding of C_{70}-Met and C_{70}-Cys adducts to DNA, the values of binding constants were calculated: $K_b = 9.76 \pm 0.27 \times 10^6$ M^{-1} for C_{70}-Met and $K_b = 9.42 \pm 0.34 \times 10^6$ M^{-1} for C_{70}-Cys. Literature analysis reveals that the binding constants of such fullerene adducts as C_{60}-Gly ($C_{60}(C_2NH_4O_2)_4H_4$)[20] $K_b = 9.85 \pm 0.65 \cdot 10^6$ M^{-1}, C_{70}-Thr ($C_{60}(C_4H_9NO_3)_2$)[66] $K_b = 9.54 \pm 0.49 \cdot 10^6$ M^{-1}, and C_{60}-Hyp ($C_{60}(C_5H_9NO_3)_2$)[48] $K_b = 5.70 \pm 0.42 \cdot 10^6$ M^{-1} are of the same order. It can be concluded that in the case of fullerene adducts, a rather strong interaction with DNA is observed.

3.4.3. Binding of C_{70} Adducts to HSA. Figure 16 shows the dependence of the thermal effect of the interaction of C_{70}-Met and C_{70}-Cys with HSA depending on the volume of the titrant at T = 298.5 *K*. Using the experimental data, based on the thermodynamic model of independent binding, the thermodynamic parameters of C_{70}-adduct binding with HSA were calculated.[86]

https://doi.org/10.1021/acs.jced.5c00615
J. Chem. Eng. Data XXXX, XXX, XXX−XXX

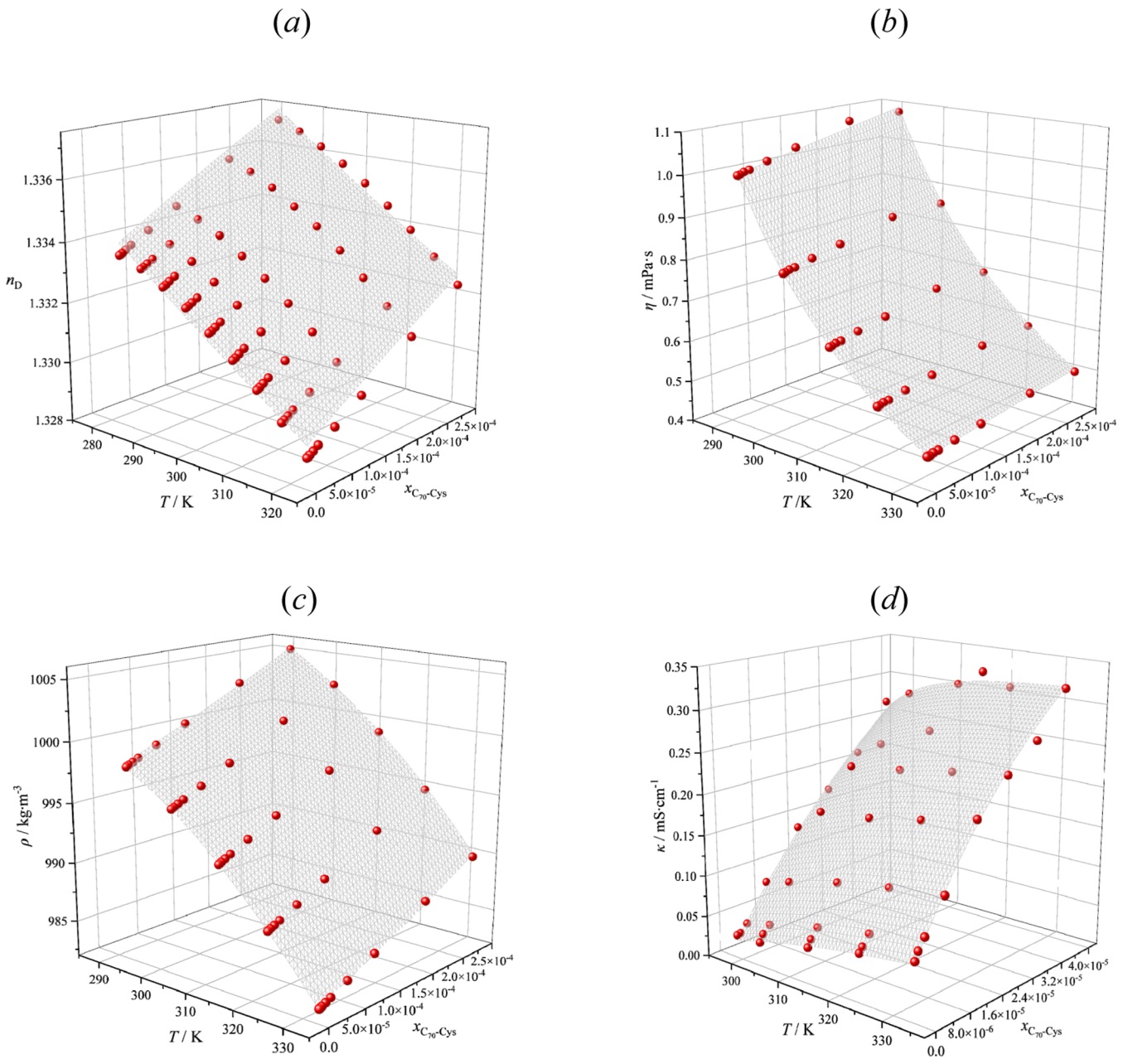

Figure 13. *T-C* dependences of refraction indices (*a*), viscosities (*b*), densities (*c*), and electrical conductivities (*d*) of C_{70}-Cys aqueous solutions; red spheres are experimental data, surfaces are calculated data.

The interpolation was performed using the independent binding model in NanoAnalyze Data Analysis software version 3.6.0 of a Nano ITC 2G Isothermal Titration Microcalorimeter. The Weissmann equation was used to calculate the binding constant from calorimetric titration data.[87] The stoichiometry values of the interaction show that one molecule of adduct binds to two molecules of HSA; the thermodynamic characteristics of the interaction of fullerene adducts are presented in Table 12. The obtained binding constants of HSA with C_{70} fullerene adducts (K_b = 2.2 × 10^6 M^{-1} for C_{70}-Met and K_b = 2.9 × 10^6 M^{-1} for C_{70}-Cys) are in the effective range of 10^4–10^6 mol·dm^{-3}, which is necessary for HSA to perform its transport function in the bloodstream.[88] In turn, at lower values of the binding constant, the complexes would not be strong enough; at higher values, irreversible binding would occur and the adduct would not be released from the complex with HSA.[88]

The results of HSA binding energies to C_{70}-Cys and C_{70}-Met at sites IA, IIA, IIIA, IB, IIB, and IIIB and the corresponding docking scores are summarized in Table 13. During the docking process, it was found that there was only one preferred pose of C_{70}-Cys and C_{70}-Met for each HSA binding site (Figure S15).

According to the ΔG values of MM-GBSA binding, the C_{70}-Met ligand binds best to site IIIB and the worst binding was demonstrated for site IIB; in turn, the C_{70}-Cys ligand binds best to site IIIB and the worst binding was demonstrated for site IIA (see Table 13).

The C_{70}-Met binding study showed the following: (i) in site IIA O2145 and O2141 atoms of Glu292 formed hydrogen bonds with H130, H129, H111 atoms of carboxyl and imino

https://doi.org/10.1021/acs.jced.5c00615
J. Chem. Eng. Data XXXX, XXX, XXX−XXX

Table 10. Total Energies, HOMO and LUMO Values for C_{70}-Met and C_{70}-Cys Adducts with Saturn-Like Distribution of Amino Acid Residues Extrapolated to T = 0 K[a,b]

Isomer	(1)	(2)	(3)	(4)	(5)
C_{70}-Met	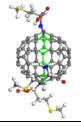	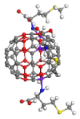	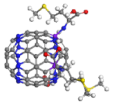	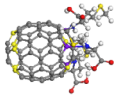	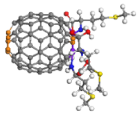
Total energy (Ha)	-5065.267	-5065.406	-5065.368	-5065.419	-5065.399
HOMO (eV)	-4.899	-5.256	-5.241	-5.108	-5.165
LUMO (eV)	-4.502	-4.150	-3.958	-3.855	-3.841
C_{70}-Cys	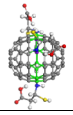	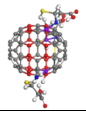	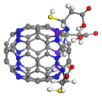	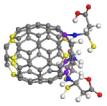	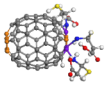
Total energy (Ha)	-4829.679	-4829.801	-4829.770	-4829.818	-4829.770
HOMO (eV)	-4.988	-5.299	-5.328	-5.080	-5.171
LUMO (eV)	-4.598	-4.186	-3.940	-3.839	-3.837

[a]As can be seen from Table 10, the structures of isomers #1, 2, 3, and 5 are the least favorable. [b](1) is the equatorial distribution, (2) is the distribution of residues on the outer part of the equatorial belt, (3) is the distribution of residues on one carbon atom belt away from the outer part equatorial, (4) is the distribution of residues on the almost terminal part of the fullerene core, (5) is the distribution of residues on the terminal part of the fullerene core.

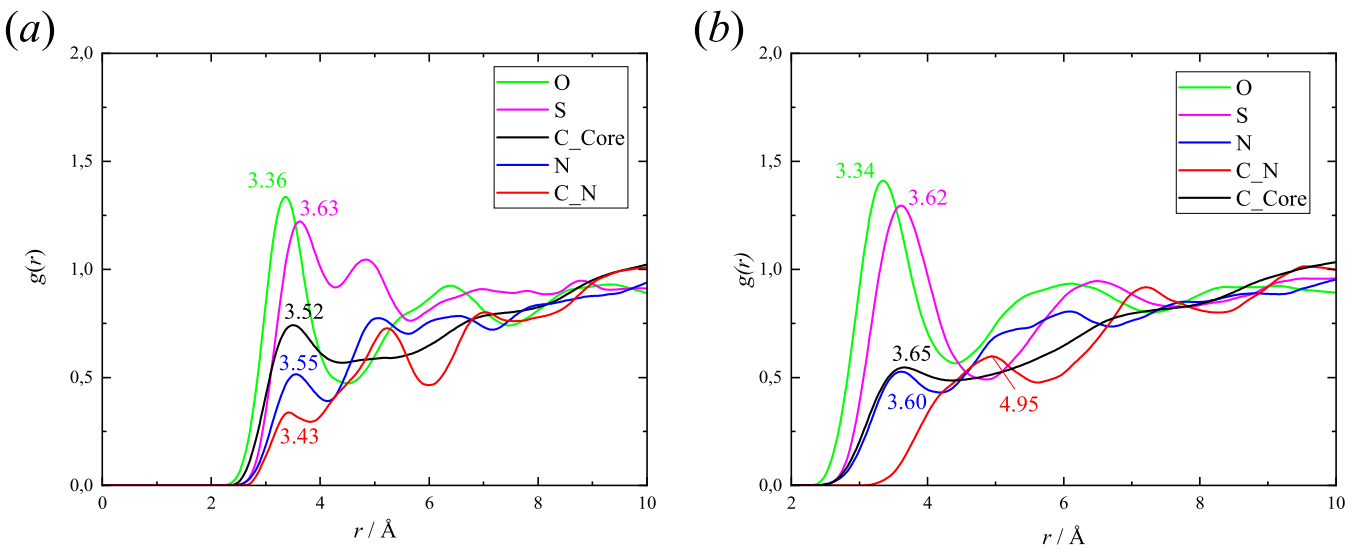

Figure 14. Radial distribution functions between the C_{70}-Met (*a*) and C_{70}-Cys (*b*) atoms and the oxygen atoms of water.

groups of L-Met; the H5710 atom of Arg218 formed a hydrogen bond with the O100 atom of the carboxyl group of L-Met; (ii) in site IIIA the O2820 atom of Gln390 formed a hydrogen bond with the H91 atom of the carboxyl group of L-Met; the O2763 atom of Glu383 and O3565 atom of Ser489 formed hydrogen bonds with the H130 and H111 atoms of imino groups of L-Met; the H6918 atom of Lys414 formed a hydrogen bond with the O99 atom of L-Met; (iii) in site IB the O1105 atom of Glu141 formed a hydrogen bond with the H91 atom of the carboxyl group of L-Met; the H5685 atom of Arg145 formed a hydrogen bond with the O80 atom of the carboxyl group of L-Met; the N1065 atom of Lys137 formed π-cation bonds with the fullerene core; the O869 atom of Arg114 formed a hydrogen bond with the H110 atom of the carboxyl group of L-Met; (*iv*) in site IIB Phe206 formed a $\pi-\pi$ stacking with the fullerene core; O2803 and O2802 atoms of Glu354 formed a bond with H91 and H129 atoms of the carboxyl group of L-Met; (v) in site IIIB the O4415 atom of Gln580 and O3824 atom of Lys500 formed hydrogen bonds with H129 and H110 atoms of the L-Met carboxyl group; hydrogen atoms of Phe502 formed bonds with O100 and O81 atoms of the L-Met carboxyl group.

The C_{70}-Cys binding study to HSA showed the following: (i) in site IIA the H5748 atom of Arg218 and H5711 atom of Arg222 formed hydrogen bonds with the O2141 atom of the carboxyl group of L-Cys; the H5536 atom of Lys195, O2145

https://doi.org/10.1021/acs.jced.5c00615
J. Chem. Eng. Data XXXX, XXX, XXX−XXX

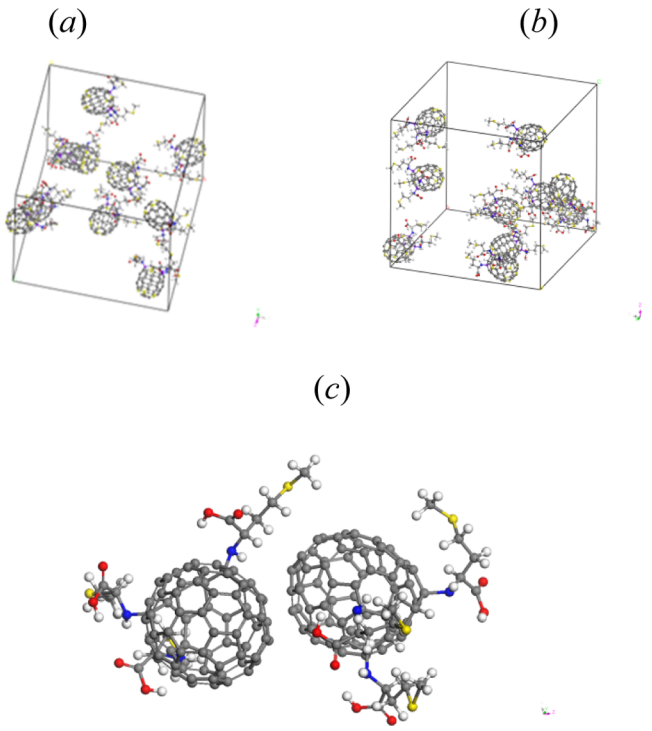

Figure 15. Initial (*a*) configurations and final (*b*) configurations of the C_{70}-Met−H_2O binary system during MD simulation; visualization of the C_{70}-Met molecules' association in the aqueous solution (*c*).

Table 11. Values of Apparent Rate Constants of DPPH Reduction by Various Fullerene Adducts (k_1 is the Fast Stage, k_2 is the Slow Stage) at 298.15 K

adduct	$k_1 \cdot 10^{-3}/\text{min}^{-1}$	$k_2 \cdot 10^{-3}/\text{min}^{-1}$	ref
C_{70}-Met	6.50 ± 0.90	3.16 ± 0.10	this work
C_{70}-Cys	7.60 ± 0.10	3.39 ± 0.20	this work
C_{70}-Thr	11.20 ± 0.60	1.27 ± 0.04	66
C_{60}-Gly	3.52 ± 0.28	1.12 ± 0.03	20
C_{60}-Hyp	8.35 ± 0.15	1.31 ± 0.04	48
C_{60}-Arg	15.10 ± 0.17	3.80 ± 0.02	85

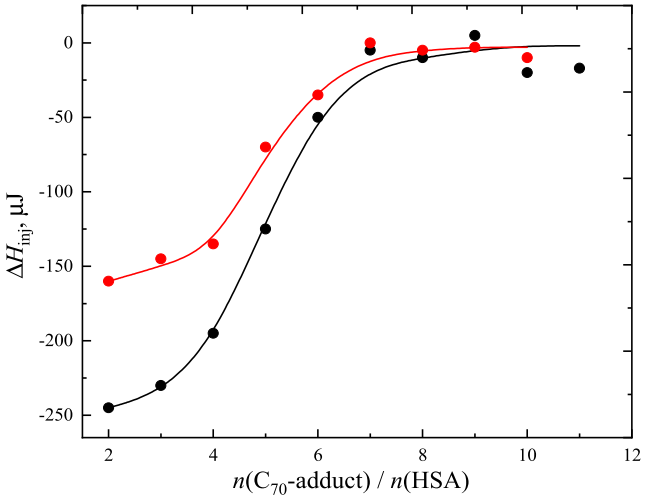

Figure 16. Dependence of the thermal effect of the reaction between C_{70}-Met (black), C_{70}-Cys (red), and HSA at T = 298.15 κ, $n(C_{70}$-adduct$)/n$(HSA) is the molar ratio of the C_{70}-adduct to HSA.

atom of Glu292, O1334 atom of Glu184 formed bonds with O90, H83, H111 atoms of the carboxyl group of L-Cys; Glu188 formed a hydrogen bond with the hydrogen atom of the thiol group of L-Cys; the N3767 atom of Lys436 formed a π-cation bond with the fullerene core; Glu292 formed a bond with the H96 atom of the imino group of L-Cys; (ii) in site IIIA the O2763 atom of the carboxyl group of Glu383 formed a hydrogen bond with the H96 atom of the L-Cys; the O3566 atom of Ser489 formed a hydrogen bond with the H110 atom of the L-Cys; the O3572 atom of Ala490 formed hydrogen bonds with H83 of the L-Cys carboxyl group; the O3589 atom of Glu492 formed a hydrogen bond with the H81 atom of the carboxyl group of the L-Cys and the H111 atom of the L-Cys thiol group; (iii) in site IB the N1065 atom of Lys137 formed a π-cationic bond with the fullerene core; the O1032 atom of Phe134 formed a bond with the H97 atom of the carboxyl group of L-Cys; the H5685 atom of Arg145 formed a bond with the O105 atom of the carboxyl group of L-Cys; the O869 atom of Arg114 formed a hydrogen bond with the H81 atom of the thiol group of L-Cys; (iv) in site IIB the O2803 atom of Glu354 and O3784 atom of Glu479 formed bonds with H96 and H109 hydrogens of the thiol group of L-Cys; the H7051 atom of Lys323, H8311 atom of Ser480, and O3817 atom of Asn483 formed hydrogen bonds with O91, O105, H111 atoms of carboxyl groups of L-Cys; Phe206 formed π−π-stacking with the fullerene core; (v) in site IIIB the H8138 atom of Phe502 and O3882 atom of Phe507 are bonded to O77 and H97 atoms of the carboxyl group of L-Cys.

Figure S16 allows us to conclude that C_{70}-Met and C_{70}-Cys slightly reduce the esterase activity of HSA in the concentration range C = 3−30 μM. Literature analysis reveals that fullerene adducts have no effect on the esterase activity of HSA across the entire concentration range C = 3−24 μM.[63,65,66]

4. CONCLUSIONS

In this work, the physicochemical and biological study of aqueous solutions of the water-soluble fullerene adducts C_{70}-Met and C_{70}-Cys was conducted. It was shown that in the dilute solutions significant compression and structuring of the solutions, along with significant decrease in the values of the partial molar volumes, were observed. The data on the solubility of C_{70}-Met and C_{70}-Cys show that the synthesized adducts are compatible with water and aqueous solutions; the solubility diagrams of C_{70}-Met−NaCl−H_2O and C_{70}-Cys−NaCl−H_2O ternary systems consist of two branches corresponding to the crystallization of fullerene adducts' crystal hydrates (C_{70}-Cys·$4H_2O$ or C_{70}-Met·$4H_2O$) and NaCl as well as one invariant point corresponding to simultaneous saturation by both solid phases. It was shown that C_{70}-Met and C_{70}-Cys are weak electrolytes. The thermodynamic dissociation constant revealed that the addition of an amino acid to the C_{70} core leads to a decrease in the acidity of the carboxyl group. C_{70}-Met and C_{70}-Cys are the surface-active substances; thus, associates of different sizes were adsorbed on the surface layer depending on the concentration. $\lg P_{ow}$ shows that adducts have the same affinity for both phases. The fullerene adduct solutions are strongly associated, at the same time, depending on the concentration, first-order associates with sizes of tens of nanometers, second-order associates with sizes of hundreds of nanometers, and third-order associates with sizes of 1−2 μm were formed. Using the VD−AS model, the activity coefficients of fullerene

https://doi.org/10.1021/acs.jced.5c00615
J. Chem. Eng. Data XXXX, XXX, XXX−XXX

Table 12. Thermodynamic Characteristics of the Interaction of C_{70}-Met and C_{70}-Cys with HSA at T = 298.15 K[a,b]

adduct	K_d,M^{-1}	n	ΔH, kJ·mol^{-1}	ΔS,J·mol^{-1}·K^{-1}	ΔG, kJ·mol^{-1}	$T\Delta S$, kJ·mol^{-1}	K_b,M^{-1}
C_{70}-Met	4.6×10^{-7}	0.36 ± 0.05	−51.15 ± 1.51	−50.20 ± 4.72	−36.18 ± 3.23	−14.96 ± 1.43	2.2×10^{6}
C_{70}-Cys	3.5×10^{-7}	0.36 ± 0.05	−32.69 ± 1.52	13.88 ± 2.70	−37.09 ± 3.56	4.14 ± 0.41	2.9×10^{6}

[a]Literature analysis reveals that the values of the binding constants of the fullerene adducts (C_{60}-Arg ($C_{60}(C_6H_{13}N_4O_2)_8H_8$)[85] K_b =·1.48 ± 0.04·10^5 M^{-1}, C_{70}-Thr ($C_{60}(C_4H_9NO_3)_2$)[66] K_b =·3.31 ± 0.03·10^5 M^{-1}, and C_{60}-Hyp ($C_{60}(C_5H_9NO_3)_2$)[48] K_b =·1.29 ± 0.03·10^5 M^{-1}) to HSA are in the effective range, which is necessary to perform its transport function. [b]K_d is the dissociation constant, K_b is the binding constant, n is the stoichiometric coefficient, ΔH, ΔS, ΔG are changes of enthalpy, entropy, and Gibbs energy of C_{70} adducts interaction with HSA, T is the absolute temperature.

Table 13. Docking Results for Top Poses of C_{70}-Met and C_{70}-Cys Molecules and the Corresponding MM-GBSA Binding Energies at Different Sites of HSA

site	IIA	IIIA	IB	IIB	IIIB
		C_{70}-Met			
ΔG of binding (MM-GBSA), kcal·mol^{-1}	−41.51	−43.83	−58.16	−31.50	−61.13
XP (GScore), kcal·mol^{-1}	−5.90	−6.01	−6.28	−5.69	−6.94
		C_{70}-Cys			
ΔG of binding (MM-GBSA), kcal·mol^{-1}	−29.34	−51.61	−59.74	−37.53	−59.77
XP (GScore), kcal·mol^{-1}	−6.46	−6.29	−7.24	−6.83	−7.18

adducts in aqueous solutions and concentrations corresponding to the loss of thermodynamic stability were calculated. It was found that the loss of thermodynamic stability corresponds to the formation of third-order associates in the studied binary systems. Using the calorimetric titration method, the thermodynamic parameters of the binding of C_{70}-Met and C_{70}-Cys with HSA were calculated; the obtained values of binding constants indicate that HSA can perform a transport function in the bloodstream. The computer modeling showed that both adducts preferentially bind to the IIIB site of HSA. In addition, it was determined that C_{70}-Met and C_{70}-Cys formed rather strong complexes with DNA ($K_b = 9.76 \times 10^6$ M^{-1} for C_{70}-Met and $K_b = 9.42 \times 10^6$ M^{-1} for C_{70}-Cys) and exhibit pronounced antiradical activity in a model reaction with DPPH. The data obtained indicate that the C_{70}-Met and C_{70}-Cys adducts are promising nanomaterials for further application in biology and medicine.

■ ASSOCIATED CONTENT

Supporting Information

The Supporting Information is available free of charge at https://pubs.acs.org/doi/10.1021/acs.jced.5c00615.

Information pertaining to the data for C_{70}-Met and C_{70}-Cys; the activation energy of viscous flow (E_a), the entropic factor (A_s) and activation temperature (T_A); correlation parameters for the Vogel−Fulcher−Tammann equation as well as fitting parameters; graphs for characterization; and a physicochemical study (PDF)

■ AUTHOR INFORMATION

Corresponding Authors

Konstantin N. Semenov − *Pavlov First Saint Petersburg State Medical University, Saint Petersburg 197022, Russia; Institute of Chemistry, Saint Petersburg State University, 26 Universitetskii Prospect, Saint Petersburg 198504, Russia; St. Petersburg State Institute of Technology (Technical University), Saint Petersburg 190013, Russia; Kabardino-Balkarian State University Named After H.M Berbekov, Nalchik 360004 Kabardino-Balkaria, Russia;* orcid.org/0000-0003-2239-2044; Email: knsemenov@gmail.com

Vladimir V. Sharoyko − *Pavlov First Saint Petersburg State Medical University, Saint Petersburg 197022, Russia; Institute of Chemistry, Saint Petersburg State University, 26 Universitetskii Prospect, Saint Petersburg 198504, Russia; St. Petersburg State Institute of Technology (Technical University), Saint Petersburg 190013, Russia;* Email: sharoyko@gmail.com

Authors

Ali Mlhem − *St. Petersburg State Institute of Technology (Technical University), Saint Petersburg 190013, Russia;* orcid.org/0009-0007-4671-6046

Alexander V. Akentiev − *Institute of Chemistry, Saint Petersburg State University, 26 Universitetskii Prospect, Saint Petersburg 198504, Russia*

Dmitry A. Nerukh − *Department of Mathematics, Aston University, Birmingham B4 7ET, U.K.;* orcid.org/0000-0001-9005-9919

Natalia V. Petukhova − *Pavlov First Saint Petersburg State Medical University, Saint Petersburg 197022, Russia*

Kirill V. Timoshchuk − *Pavlov First Saint Petersburg State Medical University, Saint Petersburg 197022, Russia*

Yuri Anufrikov − *Institute of Chemistry, Saint Petersburg State University, 26 Universitetskii Prospect, Saint Petersburg 198504, Russia*

Gleb O. Iurev − *Pavlov First Saint Petersburg State Medical University, Saint Petersburg 197022, Russia; Institute of Chemistry, Saint Petersburg State University, 26 Universitetskii Prospect, Saint Petersburg 198504, Russia*

Andrey V. Petrov − *Institute of Chemistry, Saint Petersburg State University, 26 Universitetskii Prospect, Saint Petersburg 198504, Russia;* orcid.org/0000-0002-4650-4891

Igor V. Murin − *Institute of Chemistry, Saint Petersburg State University, 26 Universitetskii Prospect, Saint Petersburg 198504, Russia*

Nikolay A. Charykov − *Pavlov First Saint Petersburg State Medical University, Saint Petersburg 197022, Russia; St. Petersburg State Institute of Technology (Technical University), Saint Petersburg 190013, Russia*

Dilafruz K. Kholmurodova − *Scientific and practical Center of Immunology, Allergology and Human Genomics at Samarkand State Medical University, Samarkand 140100, Uzbekistan*

Dilfuza Kiyamova − *Scientific and practical Center of Immunology, Allergology and Human Genomics at Samarkand State Medical University, Samarkand 140100, Uzbekistan*

Perxan Aytmuratova − *Scientific and practical Center of Immunology, Allergology and Human Genomics at Samarkand State Medical University, Samarkand 140100, Uzbekistan*

Maftuna Esanova qizi − *Scientific and practical Center of Immunology, Allergology and Human Genomics at Samarkand State Medical University, Samarkand 140100, Uzbekistan*

Complete contact information is available at: https://pubs.acs.org/10.1021/acs.jced.5c00615

Author Contributions

Konstantin N. Semenov—Conceptualization, validation, supervision, project administration. Ali Mlhem—Investigation of phase equilibria, conducting of physicochemical calculations, measurement of electrical conductivity of aqueous solutions of fullerene adduct. Alexander V. Akentiev—Investigation of surface properties. Dmitry A. Nerukh—Investigation of association in aqueous solutions using the molecular dynamics method. Natalia V. Petukhova—Investigation of the association in aqueous solutions using the molecular dynamics method. Kirill V. Timoshchuk—Investigation of the association in aqueous solutions using the molecular dynamics method. Yuri A. Anufrikov−Measurement of temperature and concentration dependencies of viscosity, density and refraction, titration calorimetry. Gleb O. Iurev—Conducting of physicochemical calculations, writing and editing of original draft. Andrey V. Petrov—Conducting of quantum chemical calculations. Igor V. Murin—Validation, supervision. Nikolay A. Charykov—Conducting of physicochemical calculations. Dilafruz K. Kholmurodova—Conducting of physicochemical calculations. Dilfuza S. Kiyamova−Conducting of physicochemical calculations. Perxan G. Aytmuratova−Conducting of physicochemical calculations. Maftuna B. Esanova qizi−Conducting of physicochemical calculations. Vladimir V. Sharoyko—Writing (Original Draft, Editing), Project administration, Funding acquisition.

Notes

The authors declare no competing financial interest.

■ ACKNOWLEDGMENTS

The authors acknowledge Saint-Petersburg State University for a research project 125021902439−8. The equipment of the following Resource Centers of the Research Park of Saint Petersburg State University was used: Computing Centre, the Centre for Diagnostics of Functional Materials for Medicine, Pharmacology and Nanoelectronics, Magnetic Resonance Research Centre, Centre for Chemical Analysis and Materials Research, Thermogravimetric and Calorimetric Research. D. N. acknowledges the use of the HPC Midlands supercomputer funded by EPSRC, grant number EP/P020232/1; the access to HPC Call Spring 2021, EPSRC Tier-2 Cirrus Service; the access to Sulis Tier 2 HPC platform hosted by the Scientific Computing Research Technology Platform at the University of Warwick. Sulis is funded by EPSRC Grant EP/T022108/1 and the HPC Midlands + consortium. The collaboration was supported by the program H2020-MSCA-RISE-2018, project AMR-TB, Grant ID: 823922.

■ REFERENCES

(1) Wang, I. C.; Tai, L. A.; Lee, D. D.; Kanakamma, P. P.; Shen, C. K.-F.; Luh, T.-Y.; Cheng, C. H.; Hwang, K. C. C_{60} and Water-Soluble Fullerene Derivatives as Antioxidants Against Radical-Initiated Lipid Peroxidation. *J. Med. Chem.* **1999**, *42* (22), 4614−4620.

(2) Tsao, N.; Luh, T.-Y.; Chou, C.-K.; Wu, J.-J.; Lin, Y.-S.; Lei, H.-Y. Inhibition of Group A Streptococcus Infection by Carboxyfullerene. *Antimicrob. Agents Chemother.* **2001**, *45* (6), 1788−1793.

(3) Medzhidova, M. G.; Abdullaeva, M. V.; Fedorova, N. E.; Romanova, V. S.; Kushch, A. A. [In Vitro Antiviral Activity of Fullerene Amino Acid Derivatives in Cytomegalovirus Infection]. *Antibiot. Khimioter.* **2004**, *49* (8−9), 13−20.

(4) Lin, Y.-L.; Lei, H.-Y.; Wen, Y.-Y.; Luh, T.-Y.; Chou, C.-K.; Liu, H.-S. Light-Independent Inactivation of Dengue-2 Virus by Carboxyfullerene *C3* Isomer. *Virology* **2000**, *275* (2), 258−262.

(5) Andreev, I. M.; Romanova, V. S.; Petrukhina, A. O.; Andreev, S. M. Amino-Acid Derivatives of Fullerene C_{60} Behave as Lipophilic Ions Penetrating through Biomembranes. *Phys. Solid State* **2002**, *44* (4), 683−685.

(6) Yang, X. L.; Fan, C. H.; Zhu, H. S. Photo-Induced Cytotoxicity of Malonic Acid [C_{60}]Fullerene Derivatives and Its Mechanism. *Toxicol. in Vitro* **2002**, *16* (1), 41−46.

(7) Dugan, L. L.; Turetsky, D. M.; Du, C.; Lobner, D.; Wheeler, M.; Almli, C. R.; Shen, C. K.-F.; Luh, T.-Y.; Choi, D. W.; Lin, T.-S. Carboxyfullerenes as Neuroprotective Agents. *Proc. Natl. Acad. Sci. U.S.A.* **1997**, *94* (17), 9434−9439.

(8) Dugan, L. L.; Lovett, E. G.; Quick, K. L.; Lotharius, J.; Lin, T. T.; O'Malley, K. L. Fullerene-Based Antioxidants and Neurodegenerative Disorders. *Parkinsonism Relat Disord* **2001**, *7* (3), 243−246.

(9) Käsermann, F.; Kempf, C. Buckminsterfullerene and Photodynamic Inactivation of Viruses. *Rev. Med. Virol* **1998**, *8* (3), 143−151.

(10) Vileno, B.; Sienkiewicz, A.; Lekka, M.; Kulik, A. J.; Forró, L. In Vitro Assay of Singlet Oxygen Generation in the Presence of Water-Soluble Derivatives of C_{60}. *Carbon N Y* **2004**, *42* (5−6), 1195−1198.

(11) Borisenkova, A. A.; Bolshakova, O. I.; Titova, A. V.; Ryabokon, I. S.; Markova, M. A.; Lyutova, Z. B.; Sedov, V. P.; Varfolomeeva, E. Yu.; Bakhmetyev, V. V.; Arutyunyan, A. V.; Burdakov, V. S.; Sarantseva, S. V. Fullerene C_{60} Conjugate with Folic Acid and Polyvinylpyrrolidone for Targeted Delivery to Tumor Cells. *Int. J. Mol. Sci.* **2024**, *25* (10), 5350.

(12) Shi, J.; Zhang, H.; Wang, L.; Li, L.; Wang, H.; Wang, Z.; Li, Z.; Chen, C.; Hou, L.; Zhang, C.; Zhang, Z. PEI-Derivatized Fullerene Drug Delivery Using Folate as a Homing Device Targeting to Tumor. *Biomaterials* **2013**, *34* (1), 251−261.

(13) Serda, M.; Gawecki, R.; Dulski, M.; Sajewicz, M.; Talik, E.; Szubka, M.; Zubko, M.; Malarz, K.; Mrozek-Wilczkiewicz, A.; Musioł, R. Synthesis and Applications of [60]Fullerene Nanoconjugate with 5-Aminolevulinic Acid and Its Glycoconjugate as Drug Delivery Vehicles. *RSC Adv.* **2022**, *12* (11), 6377−6388.

(14) Bezmel'nitsyn, V. N.; Eletskii, A. V.; Okun', M. V. Fullerenes in Solutions. *Physics-Uspekhi* **1998**, *41* (11), 1091−1114.

(15) Bagchi, D.; Bagchi, M.; Moriyama, H.; Shahidi, F. *Bio-Nanotechnology*; Bagchi, D., Bagchi, M., Moriyama, H., Shahidi, F., Eds.; Blackwell Publishing Ltd.: Oxford, UK, 2013.

(16) Podolsky, N. E.; Marcos, M. A.; Cabaleiro, D.; Semenov, K. N.; Lugo, L.; Petrov, A. V.; Charykov, N. A.; Sharoyko, V. V.; Vlasov, T. D.; Murin, I. V. Physico-Chemical Properties of $C_{60}(OH)_{22-24}$ Water Solutions: Density, Viscosity, Refraction Index, Isobaric Heat Capacity and Antioxidant Activity. *J. Mol. Liq.* **2019**, *278*, 342−355.

(17) Ageev, S. V.; Iurev, G. O.; Podolsky, N. E.; Rakipov, I. T.; Vasina, L. V.; Noskov, B. A.; Akentiev, A. V.; Charykov, N. A.; Murin, I. V.; Semenov, K. N. Density, Speed of Sound, Viscosity, Refractive Index, Surface Tension and Solubility of $C_{60}[C(COOH)_2]_3$. *J. Mol. Liq.* **2019**, *291*, 111256.

(18) Shestopalova, A. A.; Semenov, K. N.; Charykov, N. A.; Postnov, V. N.; Ivanova, N. M.; Sharoyko, V. V.; Keskinov, V. A.; Letenko, D. G.; Nikitin, V. A.; Klepikov, V. V.; Murin, I. V. Physico-Chemical Properties of the C_{60}-Arginine Water Solutions. *J. Mol. Liq.* **2015**, *211*, 301−307.

(19) Semenov, K. N.; Charykov, N. A.; Iurev, G. O.; Ivanova, N. M.; Keskinov, V. A.; Letenko, D. G.; Postnov, V. N.; Sharoyko, V. V.;

Kulenova, N. A.; Prikhodko, I. V.; Murin, I. V. Physico-Chemical Properties of the C_{60}-L-Lysine Water Solutions. *J. Mol. Liq.* **2017**, *225*, 767−777.

(20) Sharoyko, V. V.; Ageev, S. V.; Meshcheriakov, A. A.; Podolsky, N. E.; Vallejo, J. P.; Lugo, L.; Rakipov, I. T.; Petrov, A. V.; Ivanova, A. V.; Charykov, N. A.; Semenov, K. N. Physicochemical Investigation of Water-Soluble $C_{60}(C_2NH_4O_2)_4H_4$ (C_{60}-Gly) Adduct. *J. Mol. Liq.* **2021**, *344*, 117658.

(21) Watanabe, L. A.; Bhuiyan, M. P. I.; Jose, B.; Kato, T.; Nishino, N. Synthesis of Novel Fullerene Amino Acids and Their Multi-fullerene Peptides. *Tetrahedron Lett.* **2004**, *45* (38), 7137−7140.

(22) Timofeeva, G. I.; Romanova, V. S.; Lopanova, L. A. Molecular Characteristics of Water-Soluble Fullerene Derivatives of Amino Acids and Peptides. *Russ. Chem. Bull* **1996**, *45* (4), 834−837.

(23) Timofeeva, G. I.; Tepanov, A. A.; Lopanov, V. A.; Romanova, V. S. A Study of the Behavior of Disubstituted Methyl Esters of Peptide Derivatives of Fullerene C_{60} in Aqueous Solutions. *Russ. Chem. Bull* **2012**, *61* (8), 1635−1637.

(24) Grebinyk, A.; Prylutska, S.; Buchelnikov, A.; Tverdokhleb, N.; Grebinyk, S.; Evstigneev, M.; Matyshevska, O.; Cherepanov, V.; Prylutskyy, Y.; Yashchuk, V.; Naumovets, A.; Ritter, U.; Dandekar, T.; Frohme, M. C_{60} Fullerene as an Effective Nanoplatform of Alkaloid Berberine Delivery into Leukemic Cells. *Pharmaceutics* **2019**, *11* (11), 586.

(25) Chaudhuri, P.; Paraskar, A.; Soni, S.; Mashelkar, R. A.; Sengupta, S. Fullerenol−Cytotoxic Conjugates for Cancer Chemo-therapy. *ACS Nano* **2009**, *3* (9), 2505−2514.

(26) Tishchenko, O.; Truhlar, D. G. Atom-Cage Charge Transfer in Endohedral Metallofullerenes: Trapping Atoms Within a Sphere-Like Ridge of Avoided Crossings. *J. Phys. Chem. Lett.* **2013**, *4* (3), 422−425.

(27) Valles-Pelarda, M.; Hames, B. C.; García-Benito, I.; Almora, O.; Molina-Ontoria, A.; Sánchez, R. S.; Garcia-Belmonte, G.; Martín, N.; Mora-Sero, I. Analysis of the Hysteresis Behavior of Perovskite Solar Cells with Interfacial Fullerene Self-Assembled Monolayers. *J. Phys. Chem. Lett.* **2016**, *7* (22), 4622−4628.

(28) Collado-Fregoso, E.; Hood, S. N.; Shoaee, S.; Schroeder, B. C.; McCulloch, I.; Kassal, I.; Neher, D.; Durrant, J. R. Intercalated vs Nonintercalated Morphologies in Donor−Acceptor Bulk Hetero-junction Solar Cells: PBTTT:Fullerene Charge Generation and Recombination Revisited. *J. Phys. Chem. Lett.* **2017**, *8* (17), 4061−4068.

(29) Fileti, E. E.; Chaban, V. V. Imidazolium Ionic Liquid Helps to Disperse Fullerenes in Water. *J. Phys. Chem. Lett.* **2014**, *5* (11), 1795−1800.

(30) Jiang, Y.; Zhang, H.; Cui, Z.; Tan, T. Modeling Coordination-Directed Self-Assembly of M_2L_4 Nanocapsule Featuring Competitive Guest Encapsulation. *J. Phys. Chem. Lett.* **2017**, *8* (9), 2082−2086.

(31) Guldi, D. M.; Costa, R. D. Nanocarbon Hybrids: The Paradigm of Nanoscale Self-Ordering/Self-Assembling by Means of Charge Transfer/Doping Interactions. *J. Phys. Chem. Lett.* **2013**, *4* (9), 1489−1501.

(32) Li, J.; Wang, R.; Huang, W.; Zhu, Y.; Teo, B. K.; Wang, Z. Smallest Endohedral Metallofullerenes $[Mg@C_{20}]^n$ (n = 4, 2, 0, − 2, and − 4): Endo-Ionic Interaction in Superatoms. *J. Phys. Chem. Lett.* **2023**, *14* (11), 2862−2868.

(33) Ray, A.; Liosi, K.; Ramakrishna, S. N.; Spencer, N. D.; Kuzuya, A.; Yamakoshi, Y. Single-Molecule AFM Study of DNA Damage by $^1O_2$ Generated from Photoexcited C_{60}. *J. Phys. Chem. Lett.* **2020**, *11* (18), 7819−7826.

(34) Chaban, V. V.; Fileti, E. E.; Prezhdo, O. V. Buckybomb: Reactive Molecular Dynamics Simulation. *J. Phys. Chem. Lett.* **2015**, *6* (5), 913−917.

(35) Saikia, N.; Jha, A. N.; Deka, R. Ch. Dynamics of Fullerene-Mediated Heat-Driven Release of Drug Molecules from Carbon Nanotubes. *J. Phys. Chem. Lett.* **2013**, *4* (23), 4126−4132.

(36) Giri, A.; Hopkins, P. E. Spectral Contributions to the Thermal Conductivity of C_{60} and the Fullerene Derivative PCBM. *J. Phys. Chem. Lett.* **2017**, *8* (10), 2153−2157.

(37) Wang, Q.; Jena, P. Density Functional Theory Study of the Interaction of Hydrogen with Li_6C_{60}. *J. Phys. Chem. Lett.* **2012**, *3* (9), 1084−1088.

(38) Semenov, K. N.; Meshcheriakov, A. A.; Charykov, N. A.; Dmitrenko, M. E.; Keskinov, V. A.; Murin, I. V.; Panova, G. G.; Sharoyko, V. V.; Kanash, E. V.; Khomyakov, Y. V. Physico-Chemical and Biological Properties of C_{60}-l-Hydroxyproline Water Solutions. *RSC Adv.* **2017**, *7* (25), 15189−15200.

(39) International Organization for Standardization; Guide to the Expression of Uncertainty in Measurement (GUM): Switzerland, 2004 .

(40) Semenov, K. N.; Charykov, N. A.; Murin, I. V.; Pukharenko, Y. V. Physico-Chemical Properties of the C_{60}-Tris-Malonic Derivative Water Solutions. *J. Mol. Liq.* **2015**, *201*, 50−58.

(41) Semenov, K. N.; Charykov, N. A.; Murin, I. V.; Pukharenko, Y. V. Physico-Chemical Properties of the Fullerenol-$_{70}$ Water Solutions. *J. Mol. Liq.* **2015**, *202*, 1−8.

(42) Manyakina, O. S.; Semenov, K. N.; Charykov, N. A.; Ivanova, N. M.; Keskinov, V. A.; Sharoyko, V. V.; Letenko, D. G.; Nikitin, V. A.; Klepikov, V. V.; Murin, I. V. Physico-Chemical Properties of the Water-Soluble C_{70}-Tris-Malonic Solutions. *J. Mol. Liq.* **2015**, *211*, 487−493.

(43) Semenov, K. N.; Charykov, N. A.; Meshcheriakov, A. A.; Lahderanta, E.; Chaplygin, A. V.; Anufrikov, Y. A.; Murin, I. V. Physico-Chemical Properties of the C_{60}-L-Threonine Water Solutions. *J. Mol. Liq.* **2017**, *242* (3), 940−950.

(44) Noskov, B. A.; Timoshen, K. A.; Akentiev, A. V.; Charykov, N. A.; Loglio, G.; Miller, R.; Semenov, K. N. Dynamic Surface Properties of C_{60}-Arginine and C_{60}-L-Lysine Aqueous Solutions. *Colloids Surf. A Physicochem Eng. Asp* **2017**, *529*, 1−6.

(45) Serebryakov, E. B.; Semenov, K. N.; Stepanyuk, I. V.; Charykov, N. A.; Mescheryakov, A. N.; Zhukov, A. N.; Chaplygin, A. V.; Murin, I. V. Physico-Chemical Properties of the C_{70}-l-Lysine Aqueous Solutions. *J. Mol. Liq.* **2018**, *256*, 507−518.

(46) Serebryakov, E. B.; Zakusilo, D. N.; Semenov, K. N.; Charykov, N. A.; Akentiev, A. V.; Noskov, B. A.; Petrov, A. V.; Podolsky, N. E.; Mazur, A. S.; Dul'neva, L. V.; Murin, I. V. Physico-Chemical Properties of C_{70}-L-Threonine Bisadduct ($C_{70}(C_4H_9NO_2)_2$) Aqueous Solutions. *J. Mol. Liq.* **2019**, *279*, 687−699.

(47) Sharoyko, V. V.; Ageev, S. V.; Meshcheriakov, A. A.; Akentiev, A. V.; Noskov, B. A.; Rakipov, I. T.; Charykov, N. A.; Kulenova, N. A.; Shaimardanova, B. K.; Podolsky, N. E.; Semenov, K. N. Physicochemical Study of Water-Soluble $C_{60}(OH)_{24}$ Fullerenol. *J. Mol. Liq.* **2020**, *311*, 113360.

(48) Meshcheriakov, A. A.; Iurev, G. O.; Luttsev, M. D.; Podolsky, N. E.; Ageev, S. V.; Petrov, A. V.; Vasina, L. V.; Solovtsova, I. L.; Sharoyko, V. V.; Murin, I. V.; Semenov, K. N. Physicochemical Properties, Biological Activity and Biocompatibility of Water-Soluble C60-Hyp Adduct. *Colloids Surf. B Biointerfaces* **2020**, *196*, 111338.

(49) Mikolaichuk, O. V.; Popova, E. A.; Protas, A. V.; Rakipov, I. T.; Nerukh, D. A.; Petrov, A. V.; Charykov, N. A.; Ageev, S. V.; Tochilnikov, G. V.; Zmitrichenko, I. G.; Stukov, A. N.; Semenov, K. N.; Sharoyko, V. V. A cytostatic drug from the class of triazine derivatives: Its properties in aqueous solutions, cytotoxicity, and therapeutic activity. *J. Mol. Liq.* **2022**, *356*, 119043.

(50) Semenov, K. N.; Charykov, N. A.; Kurilenko, A. V.; Keskinov, V. A.; Shaimardanov, Zh. K.; Shaimardanova, B. K.; Kulenova, N. A.; Matuzenko, M. Yu.; Klepikov, V. V. Thermodynamic Functions in the Binary System of a C_{60} Fullerene Derivative with Methionine Amino Acid−H2O. *Russ. J. Phys. Chem. A* **2020**, *94* (4), 698−703.

(51) Ceperley, D. M.; Alder, B. J. Ground State of the Electron Gas by a Stochastic Method. *Phys. Rev. Lett.* **1980**, *45* (7), 566−569.

(52) Perdew, J. P.; Zunger, A. Self-Interaction Correction to Density-Functional Approximations for Many-Electron Systems. *Phys. Rev. B* **1981**, *23* (10), 5048−5079.

https://doi.org/10.1021/acs.jced.5c00615
J. Chem. Eng. Data XXXX, XXX, XXX−XXX

(53) Perdew, J. P.; Burke, K.; Ernzerhof, M. Generalized Gradient Approximation Made Simple. *Phys. Rev. Lett.* **1996**, *77* (18), 3865−3868.
(54) Wu, Z.; Cohen, R. E. More Accurate Generalized Gradient Approximation for Solids. *Phys. Rev. B* **2006**, *73* (23), 235116.
(55) Perdew, J. P.; Ruzsinszky, A.; Csonka, G. I.; Vydrov, O. A.; Scuseria, G. E.; Constantin, L. A.; Zhou, X.; Burke, K. Restoring the Density-Gradient Expansion for Exchange in Solids and Surfaces. *Phys. Rev. Lett.* **2008**, *100* (13), 136406.
(56) Benyamini, H.; Shulman-Peleg, A.; Wolfson, H. J.; Belgorodsky, B.; Fadeev, L.; Gozin, M. Interaction of C_{60}-Fullerene and Carboxyfullerene with Proteins: Docking and Binding Site Alignment. *Bioconjug Chem.* **2006**, *17* (2), 378−386.
(57) Madhavi Sastry, G.; Adzhigirey, M.; Day, T.; Annabhimoju, R.; Sherman, W. Protein and Ligand Preparation: Parameters, Protocols, and Influence on Virtual Screening Enrichments. *J. Comput. Aided Mol. Des* **2013**, *27* (3), 221−234.
(58) Jacobson, M. P.; Pincus, D. L.; Rapp, C. S.; Day, T. J. F.; Honig, B.; Shaw, D. E.; Friesner, R. A. A Hierarchical Approach to All-Atom Protein Loop Prediction. *Proteins: Struct., Funct., Bioinf.* **2004**, *55* (2), 351−367.
(59) Jacobson, M. P.; Friesner, R. A.; Xiang, Z.; Honig, B. On the Role of the Crystal Environment in Determining Protein Side-Chain Conformations. *J. Mol. Biol.* **2002**, *320* (3), 597−608.
(60) Greenwood, J. R.; Calkins, D.; Sullivan, A. P.; Shelley, J. C. Towards the Comprehensive, Rapid, and Accurate Prediction of the Favorable Tautomeric States of Drug-like Molecules in Aqueous Solution. *J. Comput. Aided Mol. Des* **2010**, *24* (6−7), 591−604.
(61) Greenidge, P. A.; Kramer, C.; Mozziconacci, J.-C.; Wolf, R. M. MM/GBSA Binding Energy Prediction on the PDBbind Data Set: Successes, Failures, and Directions for Further Improvement. *J. Chem. Inf. Model.* **2013**, *53* (1), 201−209.
(62) Lyne, P. D.; Lamb, M. L.; Saeh, J. C. Accurate Prediction of the Relative Potencies of Members of a Series of Kinase Inhibitors Using Molecular Docking and MM-GBSA Scoring. *J. Med. Chem.* **2006**, *49* (16), 4805−4808.
(63) Kukaliia, O. N.; Ageev, S. V.; Petrov, A. V.; Kirik, O. V.; Korzhevskii, D. E.; Meshcheriakov, A. A.; Jakovleva, A. A.; Poliakova, L. S.; Novikova, T. A.; Kolpakova, M. E.; Vlasov, T. D.; Molchanov, O. E.; Maistrenko, D. N.; Murin, I. V.; Sharoyko, V. V.; Semenov, K. N. C_{60} Adduct with L-Arginine as a Promising Nanomaterial for Treating Cerebral Ischemic Stroke. *Nanomedicine* **2023**, *53*, 102698.
(64) Yang, L.-Y.; Hua, S.-Y.; Zhou, Z.-Q.; Wang, G.-C.; Jiang, F.-L.; Liu, Y. Characterization of Fullerenol-Protein Interactions and an Extended Investigation on Cytotoxicity. *Colloids Surf. B Biointerfaces* **2017**, *157*, 261−267.
(65) Sharoyko, V. V.; Shemchuk, O. S.; Meshcheriakov, A. A.; Vasina, L. V.; Iamalova, N. R.; Luttsev, M. D.; Ivanova, D. A.; Petrov, A. V.; Maystrenko, D. N.; Molchanov, O. E.; Semenov, K. N. Biocompatibility, Antioxidant Activity and Collagen Photoprotection Properties of C_{60} Fullerene Adduct with L-Methionine. *Nanomedicine* **2022**, *40*, 102500.
(66) Sharoyko, V. V.; Serebriakov, E. B.; Ageev, S. V.; Petrov, A. V.; Meshcheriakov, A. A.; Charykov, N. A.; Murin, I. V.; Maistrenko, D. N.; Molchanov, O. E.; Semenov, K. N. Biocompatibility and Biological Activity of C_{70} Fullerene Adduct with L-Threonine ($C_{70}(C_4H_9NO_3)_2$). *Biochem. Biophys. Res. Commun.* **2022**, *636*, 50−56.
(67) Abdelhalim, A. O. E.; Ageev, S. V.; Petrov, A. V.; Meshcheriakov, A. A.; Luttsev, M. D.; Vasina, L. V.; Nashchekina, I. A.; Murin, I. V.; Molchanov, O. E.; Maistrenko, D. N.; Potanin, A. A.; Semenov, K. N.; Sharoyko, V. V. Graphene Oxide Conjugated with Doxorubicin: Synthesis, Bioactivity, and Biosafety. *J. Mol. Liq.* **2022**, *359*, 119156.
(68) Abdelhalim, A. O. E.; Meshcheriakov, A. A.; Maistrenko, D. N.; Molchanov, O. E.; Ageev, S. V.; Ivanova, D. A.; Iamalova, N. R.; Luttsev, M. D.; Vasina, L. V.; Sharoyko, V. V.; Semenov, K. N. Graphene Oxide Enriched with Oxygen-Containing Groups: On the Way to an Increase of Antioxidant Activity and Biocompatibility. *Colloids Surf. B Biointerfaces* **2022**, *210*, 112232.
(69) Berdichevskiy, G. M.; Vasina, L. V.; Ageev, S. V.; Meshcheriakov, A. A.; Galkin, M. A.; Ishmukhametov, R. R.; Nashchekin, A. V.; Kirilenko, D. A.; Petrov, A. V.; Martynova, S. D.; Semenov, K. N.; Sharoyko, V. V. A Comprehensive Study of Biocompatibility of Detonation Nanodiamonds. *J. Mol. Liq.* **2021**, *332*, 115763.
(70) Semenov, K. N.; Charykov, N. A.; Arapov, O. V. Temperature Dependence of the Light Fullerenes Solubility in Natural Oils and Animal Fats. *Full., nanotubes, and carb. nanostructures* **2009**, *17* (3), 230−248.
(71) Semenov, K. N.; Mlhem, A.; Akentiev, A. V.; Nerukh, D. A.; Petukhova, N. V.; Rakipov, I. T.; Timoshchuk, K. V.; Iurev, G. O.; Petrov, A. V.; Murin, I. V.; Charykov, N. A.; Vezo, O. S.; Penkova, A. V.; Kholmurodova, D. K.; Rizaev, J. A.; Kubaev, A. S.; Sharoyko, V. V. Comprehensive Physicochemical Investigation of the Water-Soluble Adduct of C_{60} with-Methionine ($C_{60}(C_5H_{11}NO_2S)_3$): Important Data for Further Applications. *J. Chem. Eng. Data* **2025**, *70* (9), 3837−3850.
(72) Semenov, K. N.; Mlhem, A.; Akentiev, A. V.; Nerukh, D. A.; Petukhova, N. V.; Rakipov, I. T.; Timoshchuk, K. V.; Iurev, G. O.; Petrov, A. V.; Murin, I. V.; Charykov, N. A.; Kholmurodova, D. K.; Mahmudova, L. B.; Amonova, G. U.; Rabbimova, D. T.; Sharoyko, V. V. Physicochemical Properties of a Water-Soluble Adduct of C_{60} with l-Cysteine for Biomedical Applications. *J. Phys. Chem. Lett.* **2025**, *16* (36), 9453−9462.
(73) Tyurin, D. P.; Semenov, K. N.; Charykov, N. A.; Cherepkova, I. A.; Keskinov, V. A. Dissociation of Fullerenol-70-d in Aqueous Solutions and Their Electric Conductivity. *Russ. J. Phys. Chem. A* **2015**, *89* (5), 771−775.
(74) Semenov, K. N.; Letenko, D. G.; Charykov, N. A.; Nikitin, V. A.; Matuzenko, M. Yu.; Keskinov, V. A.; Postnov, V. N.; Kopyrin, A. A. Electrochemical Properties of Aqueous Solutions of Fullerenol-d. *Russ. J. Appl. Chem* **2011**, *84* (1), 79−83.
(75) Ravdel, A.; Ponomareva, A. *Brief Reference Book of Physical and Chemical Quantities*; Az-book, 2009; Vol. *11*.
(76) Kochergina, L. A.; Lytkin, A. I.; Krutova, O. N.; Damrina, K. V. Standard Enthalpies of Formation of L-glutamine and the products of its dissociation inAqueous Solution. *Russ. J. Phys. Chem. A* **2014**, *88*, 409−412.
(77) Kano, H.; Matsuo, K.; Hayashi, H.; Kato, K.; Yamakata, A.; Yamada, H.; Aratani, N. Buckyball as an Electron Donor in a Dyad of C_{60} and Xanthene Dye. *Eur. J. Org Chem.* **2021**, *2021* (23), 3377−3381.
(78) Mikulin, G. I. *Questions of Physical Chemistry of Electrolyte Solutions [Collection of Articles]; State Research and Design Institute of Basic Chemistry*; NIOKhim". - Leningrad: Chemistry. Leningrad Department, 1968.
(79) Semenov, K. N.; Kurilenko, A. V.; Charykov, N. A.; Keskinov, V. A.; Vorob'ev, A. L.; Shaimardanov, Zh. K.; Kulenova, N. A.; Onalbaeva, Zh. S.; Letenko, D. G. Solubility, Thermal Analysis, and Association of the Bis-Adducts of Light C_{60} Fullerene and Amino Acids Lysine, Threonine, and Hydroxyproline in Aqueous Solutions. *Russ. J. Phys. Chem. A* **2019**, *93* (7), 1258−1265.
(80) Cheng, T.; Zhao, Y.; Li, X.; Lin, F.; Xu, Y.; Zhang, X.; Li, Y.; Wang, R.; Lai, L. Computation of Octanol−water Partition Coefficients by Guiding an Additive Model with Knowledge. *J. Chem. Inf. Model.* **2007**, *47* (6), 2140−2148.
(81) Semenov, K. N.; Charykov, N. A.; Postnov, V. N.; Sharoyko, V. V.; Murin, I. V. Phase Equilibria in Fullerene-Containing Systems as a Basis for Development of Manufacture and Application Processes for Nanocarbon Materials. *Russ. Chem. Rev.* **2016**, *85* (1), 38−59.
(82) Semenov, K. N.; Andrusenko, E. V.; Charykov, N. A.; Litasova, E. V.; Panova, G. G.; Penkova, A. V.; Murin, I. V.; Piotrovskiy, L. B. Carboxylated Fullerenes: Physico-Chemical Properties and Potential Applications. *Prog. Solid State Chem.* **2017**, *47*−*48*, 19−36.
(83) Charykov, N. A.; Semenov, K. N.; Kurilenko, A. V.; Keskinov, V. A.; Letenko, D. G.; Kulenova, N. A.; Zolotarev, A. A.; Klepikov, V.

https://doi.org/10.1021/acs.jced.5c00615
J. Chem. Eng. Data XXXX, XXX, XXX−XXX

V. Modeling of Systems with Aqueous Solutions of UO_2^{2+} Salts. Asymmetric Model of Excess Thermodynamic Functions, Based on Virial Expansion of the Gibbs Free Energy of the Solution, VD-AS. *Radiochemistry* **2017**, *59* (2), 134−142.

(84) Delgado, A. V.; González-Caballero, F.; Hunter, R. J.; Koopal, L. K.; Lyklema, J. Measurement and Interpretation of Electrokinetic Phenomena. *J. Colloid Interface Sci.* **2007**, *309* (2), 194−224.

(85) Pochkaeva, E. I.; Meshcheriakov, A. A.; Ageev, S. V.; Podolsky, N. E.; Petrov, A. V.; Charykov, N. A.; Vasina, L. V.; Nikolaeva, O. Y.; Gaponenko, I. N.; Sharoyko, V. V.; Murin, I. V.; Semenov, K. N. Polythermal Density and Viscosity, Nanoparticle Size Distribution, Binding with Human Serum Albumin and Radical Scavenging Activity of the C_{60}-L-Arginine $(C_{60}(C_6H_{13}N_4O_2)_8H_8)$ Aqueous Solutions. *J. Mol. Liq.* **2020**, *297*, 111915.

(86) Herrera, I.; Winnik, M. A. Differential Binding Models for Isothermal Titration Calorimetry: Moving beyond the Wiseman Isotherm. *J. Phys. Chem. B* **2013**, *117* (29), 8659−8672.

(87) Turnbull, W. B.; Daranas, A. H. On the Value of c: Can Low Affinity Systems Be Studied by Isothermal Titration Calorimetry? *J. Am. Chem. Soc.* **2003**, *125* (48), 14859−14866.

(88) Pochkaeva, E. I.; Anufrikov, Yu. A.; Faenkova, V. P.; Sharoyko, V. V.; Charykov, N. A.; Murin, I. V. Isothermal Calorimetric Titration of Human Serum Albumin with the Fullerene C_{60}-L-Arginine Adduct. *Russ. J. Gen. Chem.* **2019**, *89* (8), 1731−1733.

https://doi.org/10.1021/acs.jced.5c00615
J. Chem. Eng. Data XXXX, XXX, XXX−XXX